Time and space-resolved quantification of plasma membrane sialylation for measurements of cell function and neurotoxicity

Petra Kranaster[1,2] · Christiaan Karreman[1] · Jeremias E. G. A. Dold[2,3] · Alice Krebs[1,2] · Melina Funke[1] · Anna-Katharina Holzer[1] · Stefanie Klima[1,5] · Johanna Nyffeler[1,6] · Stefan Helfrich[4,7] · Valentin Wittmann[2,3] · Marcel Leist[1,2]

Abstract

While there are many methods to quantify the synthesis, localization, and pool sizes of proteins and DNA during physiological responses and toxicological stress, only few approaches allow following the fate of carbohydrates. One of them is metabolic glycoengineering (MGE), which makes use of chemically modified sugars (CMS) that enter the cellular biosynthesis pathways leading to glycoproteins and glycolipids. The CMS can subsequently be coupled (via bio-orthogonal chemical reactions) to tags that are quantifiable by microscopic imaging. We asked here, whether MGE can be used in a quantitative and time-resolved way to study neuronal glycoprotein synthesis and its impairment. We focused on the detection of sialic acid (Sia), by feeding human neurons the biosynthetic precursor N-acetyl-mannosamine, modified by an azide tag. Using this system, we identified non-toxic conditions that allowed live cell labeling with high spatial and temporal resolution, as well as the quantification of cell surface Sia. Using combinations of immunostaining, chromatography, and western blotting, we quantified the percentage of cellular label incorporation and effects on glycoproteins such as polysialylated neural cell adhesion molecule. A specific imaging algorithm was used to quantify Sia incorporation into neuronal projections, as potential measure of complex cell function in toxicological studies. When various toxicants were studied, we identified a subgroup (mitochondrial respiration inhibitors) that affected neurite glycan levels several hours before any other viability parameter was affected. The MGE-based neurotoxicity assay, thus allowed the identification of subtle impairments of neurochemical function with very high sensitivity.

Keywords Metabolic glycoengineering · Sialic acid · Neurite integrity · Cytotoxicity · Neurotoxicity · Confocal imaging

Introduction

Examination of cellular carbohydrate metabolism allows for novel approaches to probe subtle impairments of cell function. Early identification of compounds that adversely affect the state of human neurons remains a major challenge. There are several in vitro approaches to define specific

✉ Marcel Leist
marcel.leist@uni-konstanz.de

1 In Vitro Toxicology and Biomedicine, Dept Inaugurated by the Doerenkamp-Zbinden Foundation, University of Konstanz, 78457 Konstanz, Germany

2 Konstanz Research School Chemical Biology (KoRS-CB), University of Konstanz, 78457 Konstanz, Germany

3 Department of Chemistry, University of Konstanz, 78457 Konstanz, Germany

4 The Bioimaging Center, University of Konstanz, 78457 Konstanz, Germany

5 Kooperatives Promotionskolleg (KPK) InViTe, University of Konstanz, 78457 Konstanz, Germany

6 Present Address: Environmental Protection Agency, Durham, NC, USA

7 Present Address: KNIME GmbH, 78467 Konstanz, Germany

neurotoxicity (Schmidt et al. 2017). For instance, viability measurements may be used to identify compounds that affect neurons at lower concentrations than other cell types (Culbreth et al. 2012; Leist and Jaattela 2001; Tong et al. 2017). Although they offer the possibility of high-throughput screening, viability measurements do not reveal alterations caused by compounds at sub-cytotoxic concentrations. In this case, neuron-specific morphologic endpoints such as neurite outgrowth (for developing neurons) (Ceresa et al. 2014; Delp et al. 2018b; Flaskos et al. 2011; Frimat et al. 2010; Krug et al. 2013; Stiegler et al. 2011; Wu et al. 2016) or neurite integrity (for mature neurons) (Axelsson et al. 2006; Krug et al. 2013; Saxena and Caroni 2007) can be measured and quantified. If compounds display neurotoxicity based on these endpoints, at concentrations lower than those which produce cytotoxic effects, they can be considered as potentially neurotoxic. However, due to the neuronal plasticity and functional reserve capacity, it is likely that some subtle neurotoxic effects may not manifest as gross morphological changes at the time of exposure. For this reason, functional readouts such as altered metabolism (Delp et al. 2018b) or altered signaling (Leist and Nicotera 1998) are required.

A variety of sugars (linked to lipids and proteins; having a diversity of chain lengths and branching) is forming the so-called cellular glycocalyx. It reflects the cell's physiological state and it changes upon subtle changes of cellular metabolism. (Lau et al. 2007; Ohtsubo and Marth 2006). For instance, the glycocalyx is affected by the activity of the cell's secretory pathway (Aebi et al. 2010; Dennis et al. 2009; Hebert et al. 2005). Observing cell membrane glycosylation may serve as an important quality check of a functional biosynthetic pathway. The role of some glycans is often determined by the sugars found at the outermost ends of their chains—sialic acids (Sia). These nine-carbon backbone, negatively charged sugars, play particularly important roles in the nervous system, where they regulate neurite development, regeneration, and synaptic plasticity (Schnaar et al. 2014). The vertebrate brain has a rich content of Sia-bearing glycosphingolipids—the gangliosides. These carry ~ 75% of the brain's Sia, with the remaining ~ 25% making up sialoglycoproteins (Schnaar et al. 2014; Yoo et al. 2015). Despite their importance, the functions of neuronal Sia are yet to be fully explored as they are not easily accessible to conventional molecular imaging approaches.

A method that makes the visualization of glycans possible exploits substrate flexibilities of the cellular biosynthetic machinery, i.e. the acceptance of non-natural modified sugars by some carbohydrate metabolizing enzymes. This technology, termed 'metabolic glycoengineering' (MGE), incorporates monosaccharides with a unique chemical functionality (reporter) into glycoconjugates of living cells (Campbell et al. 2007; Dube and Bertozzi 2003; Keppler

et al. 2001). In these cases, the tagged sugars (e.g. modified Sia) are positioned at the same site and with the same chemical connections as their natural counterpart (Sia) in a non-modified cell. MGE substrates have been developed to be used in a highly specific way by mammalian cells to substitute N-acetylglucosamine (GlcNAc), N-acetylgalactosamine (GalNAc), fucose, Sia or O-linked N-acetyl-glucosamine (O-GlcNAc) (Campbell et al. 2007; Dold et al. 2017; Doll et al. 2016; Du et al. 2009; Niederwieser et al. 2013; Nischan and Kohler 2016). For instance, N-acetyl-mannosamine (ManNAc) with an azide (Az) modification (N-azidoacetylmannosamine (ManNAz)) is converted within cells to azide-modified Sia (SiaAz). This sugar derivative is incorporated instead of the endogenous natural Sia and has a reporter function due to its reactive chemical functionalization (Laughlin and Bertozzi 2007). The Az-group of the protein or lipid-bound Sia can react with a chemical probe in a way that no other biological structure is affected (= bio-orthogonal reaction). In this way, only the metabolically labeled glycans (containing the reporter) are selected for the reaction (Sletten and Bertozzi 2009). The chemical reaction between the reporter and a labeled probe can be performed without compromising cell viability. The most common reaction types used for this purpose [e.g. click reactions, inverse-electron-demand Diels–Alder reaction, copper-free strain-promoted azide–alkyne cycloaddition (SPAAC)] do not affect chemical groups normally found in living cells. The MGE labeling is well tolerated by many cell lines and it can also be applied to rodent neuronal cells (Buttner et al. 2002; Merzaban et al. 2015; Schmidt et al. 1998; Vogt et al. 2012). In cells of the nervous system, MGE has been used to study the polysialylation (PSA) of the neural cell adhesion molecule (NCAM) (Charter et al. 2000, 2002; Kang et al. 2015). There is still a dearth of studies characterizing overall sialylation of proteins plus lipids on neuronal/neurite membranes (general glycocalyx biology). Moreover, hardly anything is known about changes of sialylation in pathophysiological situations such as toxicant stress (glycocalyx toxicology).

Here, we studied the metabolic incorporation of an azide-tagged sugar precursor ($Ac_4ManNAz$) as Az–Sia into the glycocalyx of mature human neurons (LUHMES). These cells (Scholz et al. 2011) are a frequently used model for human neurotoxicity (Delp et al. 2018b, 2019; Efremova et al. 2017; Ganjam et al. 2019; Harris et al. 2018; Krug et al. 2013; Singh et al. 2018; Skirzewski et al. 2018; Stiegler et al. 2011; Tong et al. 2018). We asked the question on whether the sialylation capacity can be used as an early functional readout of neurotoxicity. We optimized MGE neuronal labeling, time resolution, and signal sensitivity and implemented an imaging algorithm that allows for a simultaneous quantification of neuronal viability, neurite integrity, and MGE Sia incorporation into neuronal projections.

Testing the effect of several model compounds and toxicants revealed that the incorporation of MGE Sia into LUHMES neurites can serve as a highly sensitive assay to identify subtle neuronal changes at much earlier time points compared to other viability assays.

Material and methods

Chemicals and antibodies

Dibutyryl-cAMP (cAMP), fibronectin, Hoechst (H-33342), tetracycline, antimycin A, brefeldin A, bortezomib, colchicine, MPP+, deguelin, rotenone and tunicamycin were purchased from Sigma (Steinheim, Germany). Recombinant human fibroblast growth factor 2 (FGF-2) and recombinant human glial cell line-derived neurotrophic factor (GDNF) were purchased from R&D Systems (Minneapolis, USA). Tween-20 and sodium dodecyl sulfate (SDS) were purchased from Roth (Karlsruhe, Germany). All cell culture reagents were purchased from Gibco/Fisher Scientific (Hampton, New Hampshire, USA) unless otherwise specified. Pierce ECL Western Substrate, Streptavidin-Alexa Fluor 488, calcein-AM (AM = acetoxymethyl), CellTrace™ Calcein Red–Orange, Glyceraldehyde 3-phosphate dehydrogenase (GAPDH) monoclonal antibody ZG003 and donkey anti-rabbit IgG Alexa Fluor 555 secondary antibody were from Thermo Fisher Scientific (Waltham, Massachusetts, US). Dibenzylcyclooctyne-PEG$_4$-biotin (DBCO-biotin) conjugate was from Jena Bioscience (Jena, Germany). Neutral-buffered formalin was from Leica Biosystems (Wetzlar, Germany), peroxidase AffiniPure goat anti-mouse IgG from Jackson Immunoresearch (Cambridge, UK), mouse anti-polysialic acid NCAM antibody clone 2-2B and rabbit anti-neural cell adhesion molecule polyclonal antibody from Merck Millipore (Burlington, Massachusetts, United States), goat anti-biotin mouse antibody was from Cell Signaling Technology (Danvers, Massachusetts, USA).

Cell culture

LUHMES cells were cultured as previously described (Scholz et al. 2011). Sarstedt (Sarstedt, Nümbrecht, Germany) plastic cell culture flasks were pre-coated with 50 µg/ml PLO and 1 µg/ml fibronectin (Sigma-Aldrich, St. Louis, MO, USA) in H$_2$O overnight. Coating solution was then removed and culture flasks were washed once with H$_2$O and air-dried before cell seeding. Proliferation medium consisted of Advanced Dulbecco's modified Eagle's medium/F12, 1×N-2 supplement (Invitrogen, Karlsruhe, Germany), 2 mM L-glutamine (Gibco, Rockville, MD, USA), and 40 ng/ml recombinant human basic (FGF) (R&D Systems, Minneapolis, MN, USA). Differentiation medium consisted

of Advanced Dulbecco's modified Eagle's medium/F12, 1×N-2 supplement, 2 mM L-glutamine, 1 mM dibutyryl cAMP (Sigma-Aldrich), 1 µg/ml tetracycline (Sigma-Aldrich), and 2 ng/mL recombinant human GDNF (R&D Systems). LUHMES cells were grown at 37 °C in a humidified 95% air, 5% CO$_2$ atmosphere. Proliferating cells were enzymatically dissociated with trypsin (138 mM NaCl, 5.4 mM KCl, 6.9 mM NaHCO3, 5.6 mM D-Glucose, 0.54 mM EDTA, 0.5 g/l trypsin from bovine pancreas type-II-S; Sigma-Aldrich) and sub-cultured every 2–3 days. For differentiation, $8×10^6$ LUHMES were seeded into a T-175 flask in the proliferation medium. Differentiation started 24 h after on day 0 (d0) by changing medium to differentiation medium. After 2 days of cultivation in culture flasks, on day 2 (d2), cells were trypsinized and seeded into poly-L-ornithine (PLO)/fibronectin pre-coated plates at a cell density of $1.5×10^5$ cells/cm^2. Eight-well glass bottom ibidi-slides (Ibidi, Martinsried, Germany) used for microscopy were additionally coated with 1 mg/ml laminin (Sigma-Aldrich) by adding it to the PLO/fibronectin coating mixture. The culture medium was regularly checked for mycoplasma contamination by Venor®GeM Classic kit (Minerva Biolabs, Berlin, Germany) and LUHMES cells working stock was validated by short tandem repeat profiling. GFP–LUHMES (Schildknecht et al. 2013) and mCherry-LC3 LUHMES were cultured exactly as LUHMES cells.

Treatment with sugar derivatives

The sugar derivatives (Ac$_4$ManNAc, Ac$_4$ManNAz, Ac$_4$GalNAz, Ac$_4$GlcNAz) were synthetized following published procedures (Saxon and Bertozzi 2000; Saxon et al. 2002). The sugar stock solutions were prepared as 100 mM in DMSO and stored at −20 °C until use. Working solutions were prepared by diluting the stock solution in cell culture medium on the day of experiment. As a control, the corresponding volume of dimethylsulfoxide (DMSO) in medium was used. LUHMES cells were seeded in 96-well plates (for cytotoxicity experiments), in 8-well glass bottom ibidi µ-slides (for confocal imaging) or in 6-well plates (for western blot analysis and 1,2-diamino-4,5-methylenedioxybenzene (DMB) labeling of Sia) at the density of 150,000 cells/cm^2.

LUHMES cell surface MGE labeling and confocal imaging

Following treatment and incubation with sugar derivatives, cells were washed twice in phosphate-buffered saline (PBS) and incubated for 20 min with dibenzylcyclooctyne-PEG$_4$-biotin (DBCO-biotin) [100 µM] at 37 °C. After further two washes with PBS, cells were incubated with a mixture of streptavidin-Alexa Fluor 488 [8 µg/ml] and H-33342 [1 µg/

ml] for 20 min at 37 °C in the dark. For the NeuroGlycoTest, CellTrace™ Calcein Red–Orange [10 µM] was added to the staining mixture. Cells were then washed twice with PBS and fixed with 2% paraformaldehyde containing 4% sucrose for 10 min at room temperature (RT) in the dark. Afterward, cells were thrice washed and stored in PBS at 4 °C in the dark until imaging. For visualization, a Zeiss LSM 880 point laser scanning confocal microscope equipped with GaAsP detector and a 40×/1.40 PlanApochromat oil immersion objective (Zeiss, Oberkochen, Germany) was used. Lasers HeNe (633 nm), diode-pumped solid-state (DPSS) (561 nm), Argon (458, 488, 514 nm) and Diode 405–30 (405 nm) were used. If not otherwise indicated, five images were taken per condition as z-stack images by defining a bottom slice and imaging nine focal planes with a 0.5 µm distance in between with a total z-range of 4 µm (Suppl. Fig. S1). Images were processed using Fiji open source software.

Image-based measurement of sugar incorporation and viability with SUIKER software

For simultaneous quantification of viability, neurite area and sugar incorporation into neurites, a software tool (SUIKER) was developed (Karreman et al. 2019). Detailed description of the image analysis as well as the software itself are freely accessible at https://invitrotox.uni-konstanz.de/Suiker/. Briefly, the z-stack maximum projection images, processed using Fiji, were imported into SUIKER and the software then used the information from the fluorescent channels to detect the nucleus in the blue channel, the cytoplasm in the green channel and the MGE-labeled Sia in the red channel. First, the soma area was defined from the blue channel, excluding any background fluorescence and debris and counting in any viable as well as non-viable nuclei. The viability was determined by size exclusion of the small non-viable nuclei. By subtracting the soma area from the green cytoplasmic channel, neurite area was defined and quantified. The pixel intensities from the red channel within the neurite area were quantified giving the neurite MGE intensity readout. The software outputs were exported as Microsoft Excel file and analyzed using GraphPad Prism.

SDS-PAGE and western blot

After treatment and incubation with sugar derivatives, cells were washed twice in PBS and incubated for 20 min with DBCO-biotin [100 µM] at 37 °C. Cells were washed twice in PBS, lysed in 1×Laemmli buffer and boiled for 5 min at 95 °C. Lysates were then centrifuged for 1 min at 10,000×g using NucleoSpin Filters (Macherey–Nagel, Düren, Germany) to remove long DNA strands. Thirty-five µg of total protein were loaded on 10% SDS gels. Proteins were transferred onto nitrocellulose membranes (Amersham,

Buckinghamshire, UK) using the Invitrogen iBlot 2 system. Afterward, membranes were blocked with 5% milk (w/v) in TBS-Tween [0.1% (v/v)] for 1 h. Primary antibodies diluted in 2% milk (w/v) in TBS-Tween [0.1% (v/v)] were added onto the membranes 4 °C overnight. Membranes were then washed thrice for 10 min with TBS-Tween (0.1%) and incubated with horseradish peroxidase-conjugated secondary antibody diluted in 2% milk (w/v) in TBS-Tween [0.1% (v/v)] for 1 h at RT. After three 10 min washes with TBS-Tween (0.1%), ECL western blotting substrate (Pierce/Thermo Fisher Scientific, Rockford, IL, USA) was added for visualization. Relative band/lane intensity was quantified using a self-developed image evaluation software. Intensities were normalized to corresponding GAPDH loading control. At least three blots from independent experiments were quantified.

Specific neuronal cytotoxicity assay by high-content imaging (live cells and neurite area)

LUHMES cells, differentiated for 2 days were seeded into 96-well plates at a density of 150,000 cells/cm^2 in a volume of 90 µl of differentiation medium. Treatment with sugar precursors was applied as 10 µl of a 10× concentrated solution. The assay was then performed as described earlier (Stiegler et al. 2011). Briefly, live cells were labeled by staining solution consisting of 1 µM calcein-AM and 1 µg/ml H-33342 for 30 min at 37 °C. Afterward, cells were imaged using an automated microscope Array-Scan VTI HCS Reader (Thermo Fisher, PA, USA). Images of nuclei were taken in channel 1 (365 ± 50/461 ± 15 nm) and calcein staining was recorded in channel 2 (475 ± 40/525 ± 15 nm). An algorithm was then applied to the images that identified the neuronal somatic area based on object size, area, and intensity from channel 1. This neuronal somatic area was then expanded and subtracted from calcein area to obtain the neurite area readout. Live cells were identified as H-33342 and calcein-positive, whereas dead cells were only H-33342-positive. Both live cells and neurite area were expressed as percentage relative to control.

Immunocytochemistry

LUHMES were grown and differentiated on pre-coated 8-well glass bottom ibidi µ-slides (Ibidi, Germany) at 150,000 cells/cm^2. Cells were fixed in 4% paraformaldehyde containing 2% sucrose for 10 min at RT. Afterwards, cells were washed thrice in PBS and pre-incubated with PBS/1% bovine serum albumin (Calbiochem, San Diego, CA, USA) for 1 h at 21 °C. Then, primary antibodies were added for 1 h at RT. After three washing steps with PBS, secondary antibodies were applied for 1 h at RT in the dark. Hoechst-33342 (1 µg/mL, Molecular Probes) was added for 10 min prior to

the final washing step and cells were imaged using confocal Zeiss LSM 880 microscope as described above.

1,2-diamino-4,5-methylenedioxybenzene (DMB) labeling of Sia

LUHMES were grown and differentiated on pre-coated 6-well plates (Sarstedt, Germany) at the density of 150,000 cells/cm^2. Cells were treated on day 5 of differentiation (for 24 h treatment) and on day 6 of differentiation (for 6 h treatment) with 10 µM Ac$_4$ManNAz or DMSO as a solvent control. After corresponding treatment times were over, cells were washed twice with PBS, scraped-off the well surface, and pelleted. Afterwards, release of Sia and DMB labeling was performed as described earlier (Dold et al. 2017). Briefly, to release the Sia, each cell pellet was resuspended in 300 µl AcOH (3 M) and incubated for 90 min at 80 °C inside a thermomixer at 300 rpm. Afterwards, the mixtures were diluted in 400 µl water and 20 µl of 25% NH$_3$ in water was added to neutralize the solution. The removal of solvent was performed using a SpeedVac, washing the pellet with 200 µl EtOH thrice after each step. For DMB labeling, the pellets were dissolved in 265 µl DMB labeling solution (5.3 mM DMB·2 HCl, 16 mM Na$_2$S$_2$O$_4$, 40 mM trifluoroacetic acid (TFA) in MilliQ water). The mixture was incubated for 2.5 h at 56 °C inside a thermomixer at 300 rpm in the dark. Afterwards, the mixture was cooled for 10 min on ice and 25 µl of aqueous NaOH (0.5 M) was used for neutralization. Samples were then analyzed by analytical RP–HPLC–MS.

Data analysis

Unless otherwise noted, all data are presented as means of at least three independent experiments (i.e., using three different cell preparations). Statistical differences were tested by ANOVA with post hoc tests as appropriate, using GraphPad Prism 5.0 (GraphPad Software, La Jolla, USA).

Results

Use of MGE for incorporation of labeled Sia into cell surface glycoconjugates of human neurons

Initially, we asked whether mature human neurons are able to use an azide-tagged *N*-acetyl-mannosamine derivative (ManNAz) as precursor for the synthesis and further use of their Sia. For this reason, differentiated LUHMES cells were cultured for 24 h in the absence or presence of Ac$_4$ManNAz or its natural (non-tagged) homolog Ac$_4$ManNAc. The sugars were offered to cells in their peracetylated, membrane-permeable form. To visualize the Sia formed from ManNAz

in the neurons, they were reacted with biotin. To be able to perform this reaction on live cells (non-cytotoxic conditions, compatible with cell survival), we used a Cu(I)-free strain-promoted azide-alkyne cycloaddition (SPAAC) reaction with dibenzylcyclooctyne-PEG$_4$-biotin (DBCO-biotin) as label. The biotinylated cell surface Sia was then visualized via subsequent labeling with streptavidin-Alexa Fluor conjugates (Fig. 1a). On the cells treated with azide-tagged mannosamine (Ac$_4$ManNAz), a clear and specific signal was detected on neurites and cell bodies. No specific fluorescence was observed on untreated cells or when the cells were treated with mannosamine bearing no tag (Ac$_4$ManNAc) (Fig. 1b). These data suggest that the labeling was due to the metabolic incorporation of the synthetic sugar in cell surface (glycocalyx) carbohydrates. The neurites and cell bodies of differentiated LUHMES extend to some height (z-dimension) over the culture plate. In particular, neurites are on average closer to the bottom of a dish than the membranes around the larger cell body. Therefore, imaging of several focal planes was necessary to capture all MGE-labeled surface glycans. We found that capturing a total depth range of 4 µm did sufficiently capture MGE labeling on neurites and cell bodies (Suppl. Fig. S1). To monitor whether MGE glycans incorporate into sialic acids all over a single neuron, we used a culture containing few LUHMES stably overexpressing GFP. The mixed culture was then treated with ManNAz on day 4 and the MGE-labeled sialic acids were visualized 24 h later. The low number of GFP-LUHMES allowed us to highlight a single GFP neuron within a dense culture and to observe that the labeled glycoconjugates cover all parts of neuronal membrane, including the cell body, the neurites, and the axonal growth cone (Suppl. Fig. S2).

Sialylation does not only occur on proteins, but also on lipids (especially gangliosides). To analyze only proteins containing sialyl residues introduced by MGE, we lyzed the cells and performed western blots. The incorporated Sia were labeled with DBCO-biotin as for cytochemistry and the sialoglycoproteins were detected on the blotting membrane by an antibody against biotin. Cells labeled with DBCO-biotin, but not pre-treated with tagged sugar, served as a control for any unspecific biotin labeling. In these (negative control) samples, we observed a band of approximately 75 kDa (75,000 g/mol) (Suppl. Fig. S3). As this band also appeared in samples not treated at all with biotin, it is most likely indicating a naturally occurring biotinylated protein in LUHMES cells. Only samples from cells treated with the azide-tagged mannosamine (Ac$_4$ManNAz) showed specifically labeled protein bands (Fig. 1c).

Although mannosamine derivatives are relatively well tolerated by many cell lines (Almaraz et al. 2012; Keppler et al. 2001; Pham et al. 2015), high concentrations may be cytotoxic for susceptible cell types such as neurons (Almaraz et al. 2012; Du et al. 2009). Mature (day 5, d5)
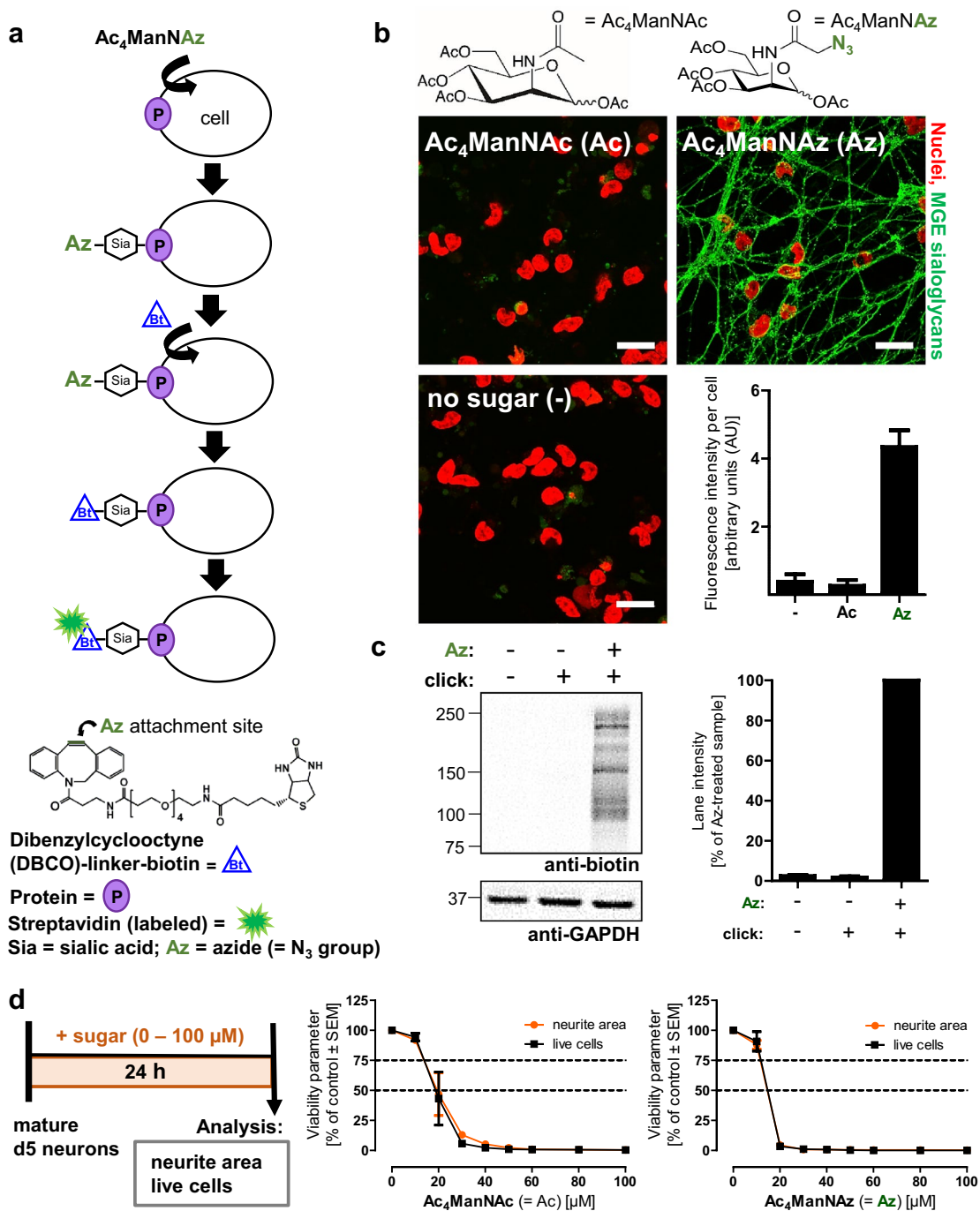
LUHMES cells were exposed to increasing concentration of the peracetylated sugars Ac$_4$ManNAc and Ac$_4$ManNAz for 24 h. Both, the neurite integrity and number of viable cells was measured and concentrations of ≥ 20 μM were found to be cytotoxic (Fig. 1d). Notably, the azide-modified sugar was not more toxic than the peracetylated natural sugar precursor. We also found that the sugars (at ≤ 100 μM) did not kill immature differentiating (day 3, d3) LUHMES cells. However, they specifically reduced

their neurite outgrowth at concentration of about ≥ 20 μM (Suppl. Fig. S4). In further control experiments, we used two alternative sugars: peracetylated N-azidoacetylgalactosamine (Ac$_4$GalNAz) and peracetylated N-azidoglucosamine (Ac$_4$GlcNAz). They showed cytotoxic potencies and specificities, very similar to the ManN-derivatives (Suppl. Fig. S4). From these data and work of others (Almaraz et al. 2012), we surmise that the acetic acid formed upon intracellular deacetylation of the sugar precursors is poorly

◂**Fig. 1** Surface labeling and quantification of neuronal sialoglyco-conjugates. **a** Graphical representation of the metabolic glycoengineering (MGE) procedure used for sialic acid (Sia) azide (Az) labeling: LUHMES cells were treated on day 5 of differentiation (d5) with Ac₄ManNAz or Ac₄ManNAc [10 μM] or left untreated. After 24 h, cells were washed and reacted for 20 min with DBCO-biotin [100 μM] followed by streptavidin-Alexa Fluor 488 [8 μg/ml]. **b** The chemical structures of the Sia precursors in their O-acetylated (OAc) cell-permeable form. The acetamide group was either unchanged (Ac) or exchanged for an N-azido-acetyl group (=Az). Representative confocal images and quantification of fluorescence intensities of LUHMES cells exposed to Ac, Az, or no sugar according to scheme **a**. Nuclei were visualized using the H-33342 dye (red). Scale bar=25 μm. **c** Western blot quantification of MGE sialoglycoproteins. LUHMES cells were treated (as described in **a**.) with 10 μM Ac₄ManNAz (=Az+) or left untreated (=Az−). On day 6 MGE sialoglycans were ligated with DBCO-biotin [100 μM] for 20 min (click+) on the intact cells, or no ligation was performed (click -). Afterwards, cell lysates were prepared and resolved by SDS-PAGE. Western blot against biotin was performed using anti-biotin antibody to detect the labeled MGE sialoglycoproteins. Quantifications represent intensities of the whole lanes, for the range of 75–250 kDa. The y axis of the gel indicates protein mass in kDa. **d** Effects of MGE sugar derivatives on neuronal viability. D5 LUHMES were treated with mannosamine analogs at concentrations 0–100 μM. After 24 h, cells were stained with calcein-AM (viable cells) and H-33342 (nuclear stain). Then, they were analyzed by a high-content screening microscope. The viability parameters are presented as live cells (black line) and neurite area (orange line). The horizontal grey dotted line indicates the 75% threshold value for cytotoxicity. Data are expressed as means±SEM from three independent biological replicates

tolerated by neurons, while the precursor sugars as such are not problematic.

As we observed that the MGE-labeled sialoglycoproteins detected by western blot always included an abundant band with an apparent molecular weight of 250 kDa, we wondered whether this corresponds to PSA–NCAM. Antibody staining showed that both NCAM, as well as the PSA colocalize on the LUHMES plasma membrane (Fig. 2a). In the brain, NCAM is by far the most abundant and therefore also the most studied PSA carrier. However, alternative PSA carrying proteins have recently also been described (Galuska et al. 2010; Muhlenhoff et al. 2013). The presence of PSA on lipids is theoretically possible, but has hitherto not been found (Fig. 2b). In LUHMES cells, the MGE–PSA found after sugar treatment, had the same size bands as detected with the PSA and NCAM antibodies (Fig. 2c). We therefore conclude that the most abundant MGE-labeled sialoglycoprotein in our LUHMES model is indeed polysialylated NCAM.

As final step of the basic characterization of MGE for human neurons, we determined what proportion of Sia was modified through MGE in LUHMES. The incorporation efficiency of the tagged Sia precursor was quantified by a 1,2-diamino-4,5-methylenedioxybenzene (DMB) labeling strategy (Dold et al. 2017). After 24 h treatment with the azide-tagged mannosamine (Ac₄ManNAz), 38%

of neuronal Sia was modified with an azide group (Fig. 3, Suppl. Fig. S5).

Overall, these experiments suggest that the azide-tagged mannosamine is successfully accepted by the LUHMES metabolism and incorporated into neuronal cell surface sialoglycans with 10 μM of the mannosamine as an adequate concentration for robust labeling without inducing neuronal cytotoxicity.

Kinetics of Sia display on LUHMES neurons

The detection and quantification of mannosamine incorporation into sialoglycans worked well, when cells were continuously grown in the presence of the Az-tagged Sia precursor for 24 h. This treatment schedule did not provide sufficient temporal resolution to allow the use of MGE efficiency as cell function endpoint. Shortening of the mannosamine uptake time before analysis of MGE glycosylated proteins and lipids would allow a clearer definition of time points at which toxicants lead to an impairment of the cellular glycoprotein processing capacity. To investigate whether the mannosamine uptake time may be shortened, d5 LUHMES cells were treated with 10 μM Ac₄ManNAz for 0.5–24 h before the sugar was washed-off from the cells. Then, control medium was added and cells were analyzed at 24 h after the start of sugar treatment (Fig. 4a). MGE sialylated protein bands were visible on western blots already after the shortest (0.5 h) treatment with mannosamine. Glycoprotein levels sufficient for a quantitative assay required labeling times of ≥ 2 h (Fig. 4b). Analysis of sugar incorporation by fluorescent imaging confirmed that a labeling time of 30 min was sufficient to visualize newly sialylated components on LUHMES plasma cell membrane. However, a time of ≥ 8 h seemed optimal for a robust and quantitative assay (Fig. 4c).

In the next set of experiments, the time point of analysis (relative to the start of label addition) was optimized. To allow for the shortest possible time windows, we re-examined label toxicity under conditions of shortened exposure. Cells were therefore treated for 0.5 h on d5 with either Ac₄ManNAc or Ac₄ManNAz at concentrations ranging from 0 to 100 μM. 24 h later (d6), viability assays based on the percentage of live cells and the neurite area measurements were performed. For both, Ac₄ManNAc as well as Ac₄ManNAz treated cells, the viability of cells remained unchanged even at the highest concentration of 100 μM (Suppl. Fig. S6a)**.** Developing neurons (d3) were slightly more sensitive, but also for these, the viability remained above the 75% cytotoxicity threshold at high (100 μM) sugar concentrations (Suppl. Fig. S6b). Shortening of the sugar uptake time, therefore allowed for an increase in sugar label concentrations up to 100 μM, without large adverse effects on neuronal viability.
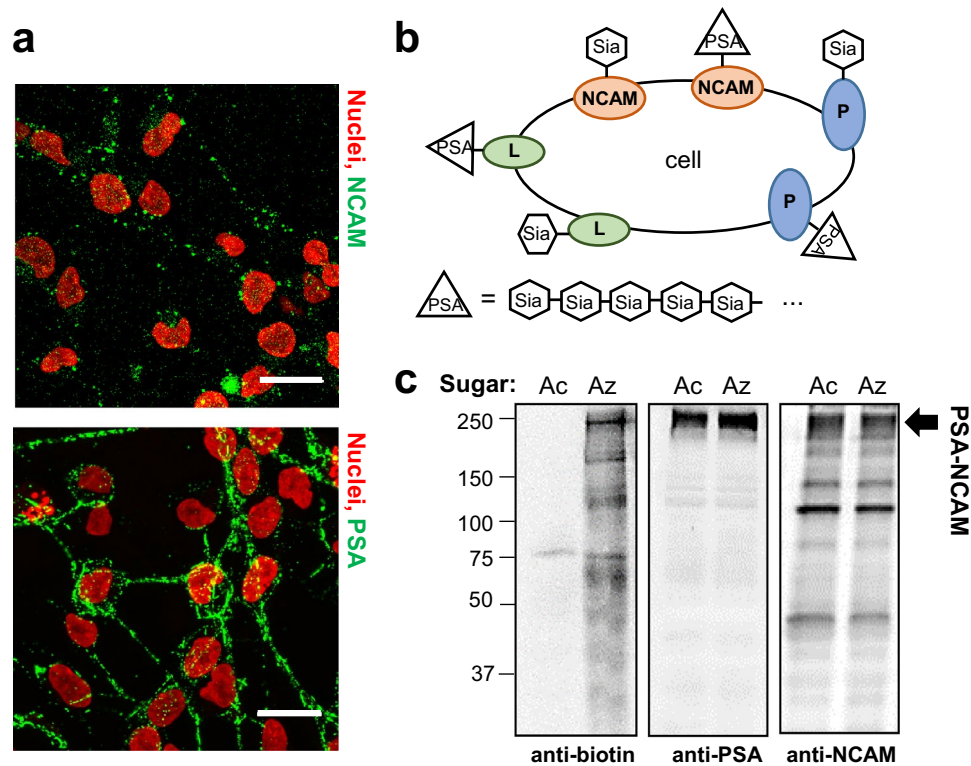
Fig. 2 Polysialic acid NCAM expression in mature LUHMES. **a** Differentiated LUHMES cells were stained on day 6 for the neural cell adhesion molecule (NCAM, green, top) or the polysialic acid NCAM (PSA, green, bottom). Nuclei were stained with H-33342 (red). Images were recorded on a confocal microscope, scale bar = 25 μm. **b** Schematic representation of cellular membrane Sia and polysialylation (P = protein; L = lipid; Sia = sialic acid; PSA = polysialic acid). **c** Representative western blot membrane images of MGE sialo- glycoproteins. LUHMES cells were treated on day 5 with 10 μM Ac$_4$ManNAz (= Az) or 10 μM Ac$_4$ManNAc (= Ac). On day 6 MGE sialoglycans were ligated with DBCO-biotin [100 μM] for 20 min on the intact cells. Afterwards, cell lysates were prepared and resolved by SDS-PAGE. Western blot was performed using anti-biotin, anti-PSA, or anti-NCAM antibody. The y axis of the gel indicates protein mass in kDa (color figure online)

Next, we asked how long neurons took to incorporate mannosamine analogs into their cell surface sialoglycoconjugates. Differentiated LUHMES were treated for 0.5 h with 100 μM Ac$_4$ManNAz. Then, the sugar was washed-off the cells and the MGE label was detected either by western blot or fluorescent imaging at 1–24 h later (Fig. 5a). The data show that the incorporation of the Az-tagged mannosamine into LUHMES sialoglycoproteins/membrane lipids took around 6–8 h (Fig. 5b, c).

In summary, adaptations of the protocol allowed for a robust MGE labeling in neurons within 6–8 h. As the cells survived the labeling procedure, it was possible to continue observation of the cells and the fate of the MGE label. We observed that the labeled Sia got internalized within few hours and mostly ended up in cellular autophagosome (Suppl. Fig. S7).

Development of a test method to quantify neurite glycoincorporation as a neuronal cell function readout

To ask whether MGE glycoincorporation can be used as a readout for neurotoxicity, we searched for stable assay conditions allowing co-treatment with tagged mannosamine and test compounds. First, incorporation times were evaluated for low innocuous sugar concentrations (10 μM), so that no additional medium change was necessary (Fig. 6a). The MGE sialoglycoprotein detection by western blot indeed showed that the labeled Sia were incorporated and detected on LUHMES glycoproteins from 6 h onwards (Fig. 6b). For fluorescent imaging, a new staining setup was developed: first, the sugar-treated live cells were ligated to DBCO-biotin; then, a staining mixture was added. This contained the streptavidin-Alexa Fluor conjugate to visualize the MGE labeling, H-33342 dye to visualize the DNA (nuclei) and CellTrace™ Calcein Red–Orange (= CellTrace), to visualize the cellular cytoplasm. The samples were then imaged

Fig. 3 Incorporation efficiency of Ac₄ManNAz into LUHMES sialic acids. **a** Day 5 LUHMES were left untreated or they were treated with 10 µM Ac₄ManNAz for 6 or 24 h to introduce the azide tag (Az) onto the sialic acids (Sia). Cells were then washed, scraped-off the culture surface and pelleted. Sia were cleaved by acetic acid [3 M] treatment at 80 °C for 90 min and subsequently labeled by 1,2-diamino-4,5-methylenedioxybenzene (DMB) for 2.5 h at 56 °C in the dark. The quinoxaline fluorophore (green) that results from the reaction of Sia and DMB was used to detect the labeled Sia. The incorporation efficiency (IE) was calculated as the DMB Az-modified Sia proportion of the total DMB labeled Sia. **b** The incorporation efficiency of the DMB-modified Az-tagged Sia after 6 and 24 h presented as a percentage of total DMB-modified Sia. **c** Az-tagged (black bars) and untagged (white bars) Sia from untreated (−) or treated (+) d5 LUHMES (as decribed in **a**). Data are means ± SEM from three biological replicates

$$\text{Incorporation efficiency (IE)} = \frac{\int \text{DMB-Sia}\textit{Az}}{\int \textit{DMB-SiaAc} + \int \textit{DMB-SiaAz}}$$
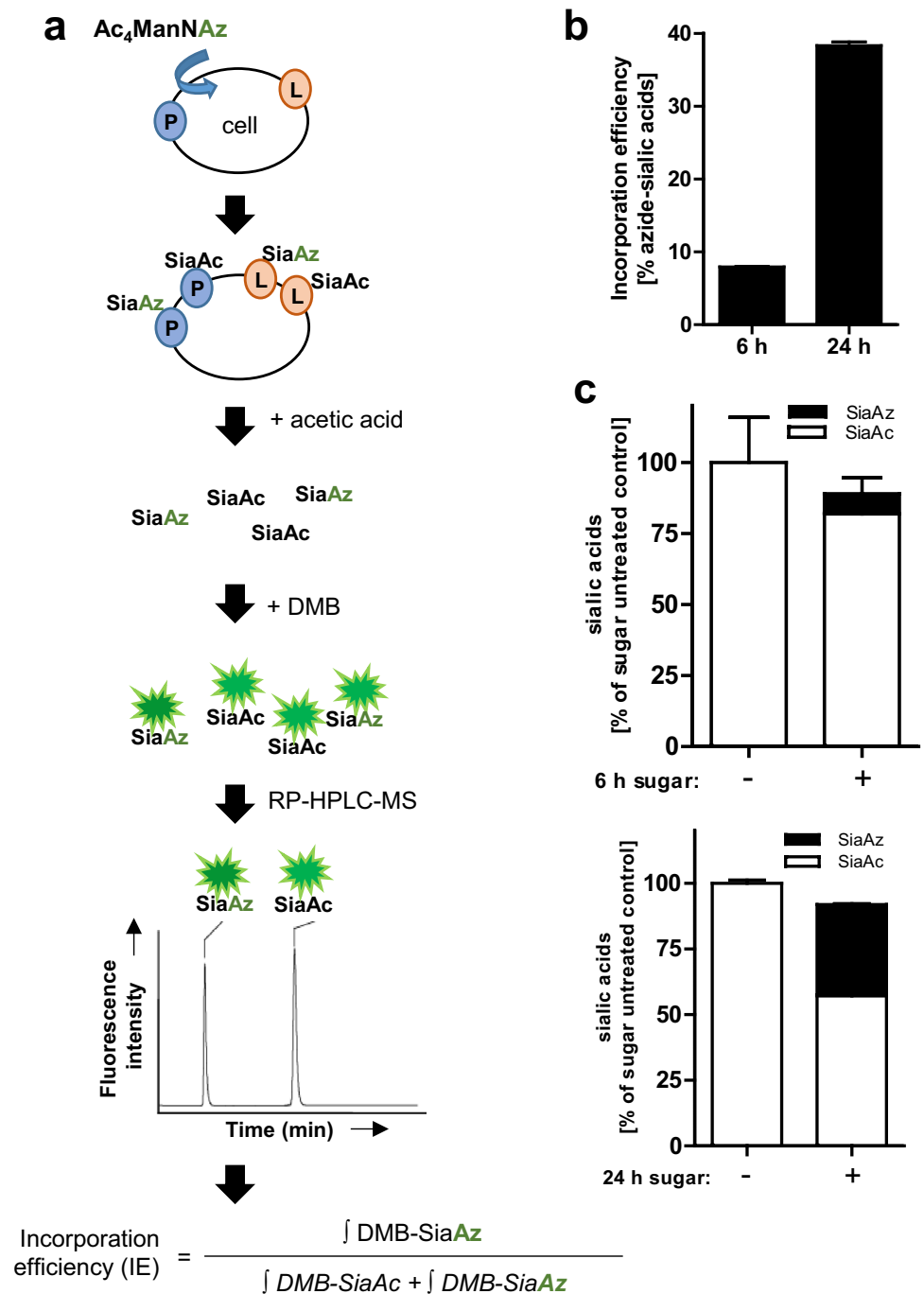
by a confocal microscope on several planes and the images were processed for each channel to maximum z-projections. For further analysis of such data, we used the image analysis program SUIKER (Karreman et al. 2019) (Fig. 6c). The program uses the nuclear stain in channel 1 (ch1, blue) to identify 'viable' and 'non-viable' nuclei based on their size and intensity (indicative of chromatin condensation and fragmentation in dying cells). From this, the viability was calculated as the percentage of live cell nuclei within the total nuclei. Then, the second channel (ch2, green) was used to quantify the total cytoplasm area of the image based on CellTrace staining. The algorithm then defined a 'neurite area' by subtracting the cell bodies (soma area) from the CellTrace positive pixels. For this, SUIKER defined the 'soma area' as the area occupied in ch1 by the nuclear stain, enlarged by an additional rim of e.g. 2 µm (parameter to be set in the program). The third channel (ch3, red) was used to quantify the metabolically labeled Sia. SUIKER determined the colocalization of ch3 positive pixels with the neurite area. The number and intensity of colocalized
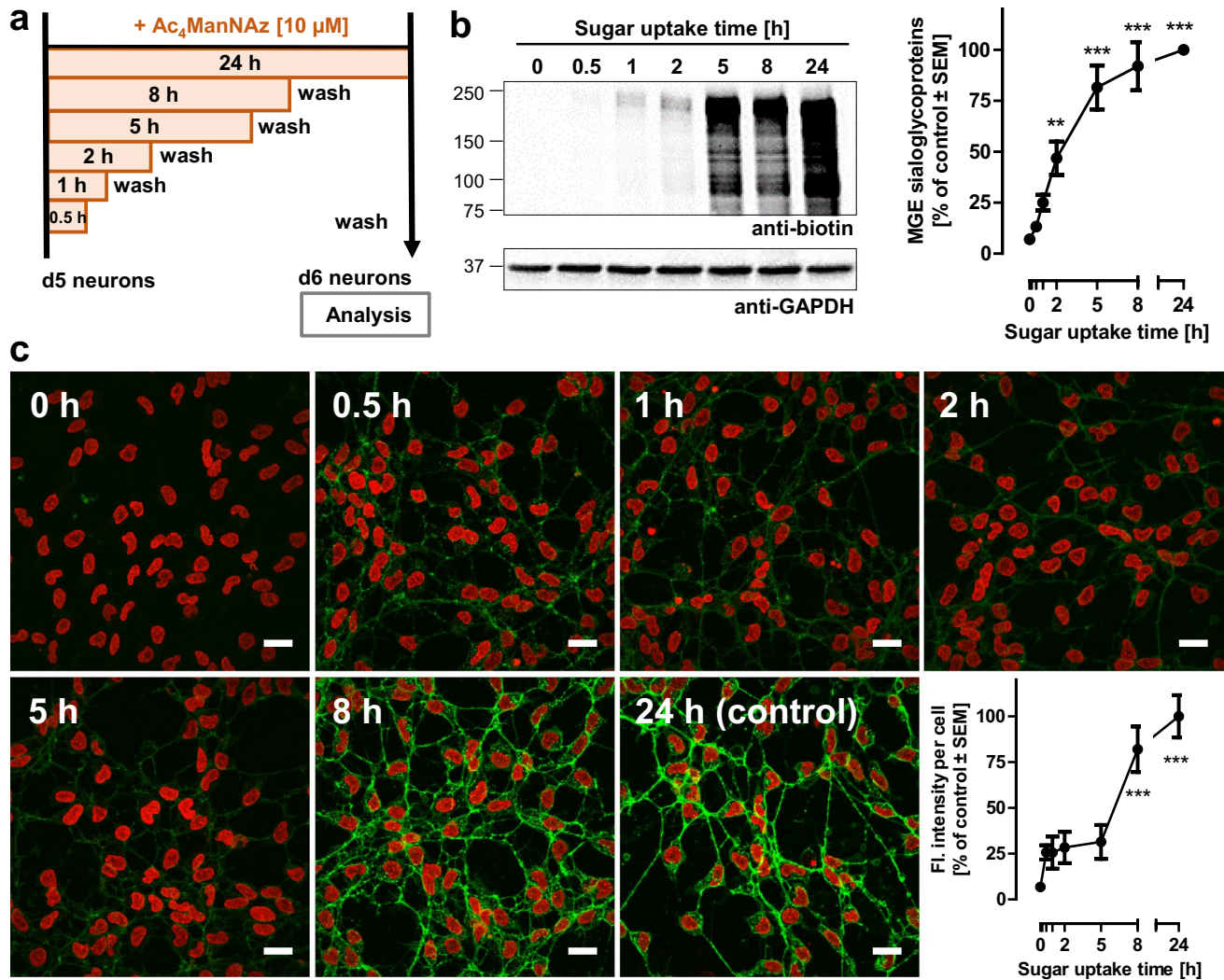
Fig. 4 Uptake kinetics of mannosamine analog's time in neurons. **a** Scheme of experimental setup. LUHMES cells were treated on d5 of differentiation with Ac$_4$ManNAz [10 μM] for 0.5–24 h or left untreated (0 h). Then, cells were washed. Labeling of MGE sialoglycans for all conditions was performed at 24 h. **b** Quantification of Ac$_4$ManNAz incorporation by western blot. Cells, labeled with DBCO-biotin [100 μM], were lysed and the homogenates were resolved by SDS-PAGE. Western blot against biotin was performed using anti-biotin antibody. For quantifications, lane intensities in the range 75–250 kDa were used. **c** Representative confocal images and their quantification displaying MGE staining intensities for different sugar treatment times. Images of nuclei stained with H-33342 (red) and MGE sialoglycans visualized by reaction via DBCO-biotin followed by Strep-AF488 (green) are merged and presented as maximum z-stack projections with a total z-range of 4 μm. Data are means ± SEM from three independent biological replicates; one-way ANOVA followed by Dunnett's test; **$p < 0.01$, ***$p < 0.001$ (all time points vs. 0 h) Scale bar = 25 μm

pixels provided the 'neurite MGE intensity' readout (Suppl. Fig. S8).

The analysis of the fluorescent images with SUIKER revealed that the cell viability remained above the 75% cytotoxicity threshold for any length of sugar treatment (1–24 h), the neurite integrity decreased to around 75% for the 8 h treatment period and was below the cytotoxicity threshold for the 24 h time point. The neurite MGE intensity increased with increasing sugar treatment time (Fig. 6d). Based on these data, we selected 6 h labeling as the ideal time to co-treat mature LUHMES with the mannosamine precursor

together with other compounds. To confirm absence of any mannosamine cytotoxicity for the 6 h incubation labeling, we tested a wide range of Ac$_4$ManNAz and Ac$_4$ManNAc concentrations (0–100 μM) for the specific test method setup (total exposure and labeling time of 6 h) and found that both viability parameters (live cells and the neurite area) remained above the 75% cytotoxicity threshold (Suppl. Fig. S9). Therefore, ideal assay conditions to test the MGE glycoincorporation during toxicant treatment (= NeuroGly-coTest) require a co-treatment of the toxicants and the sugar for 6 h.
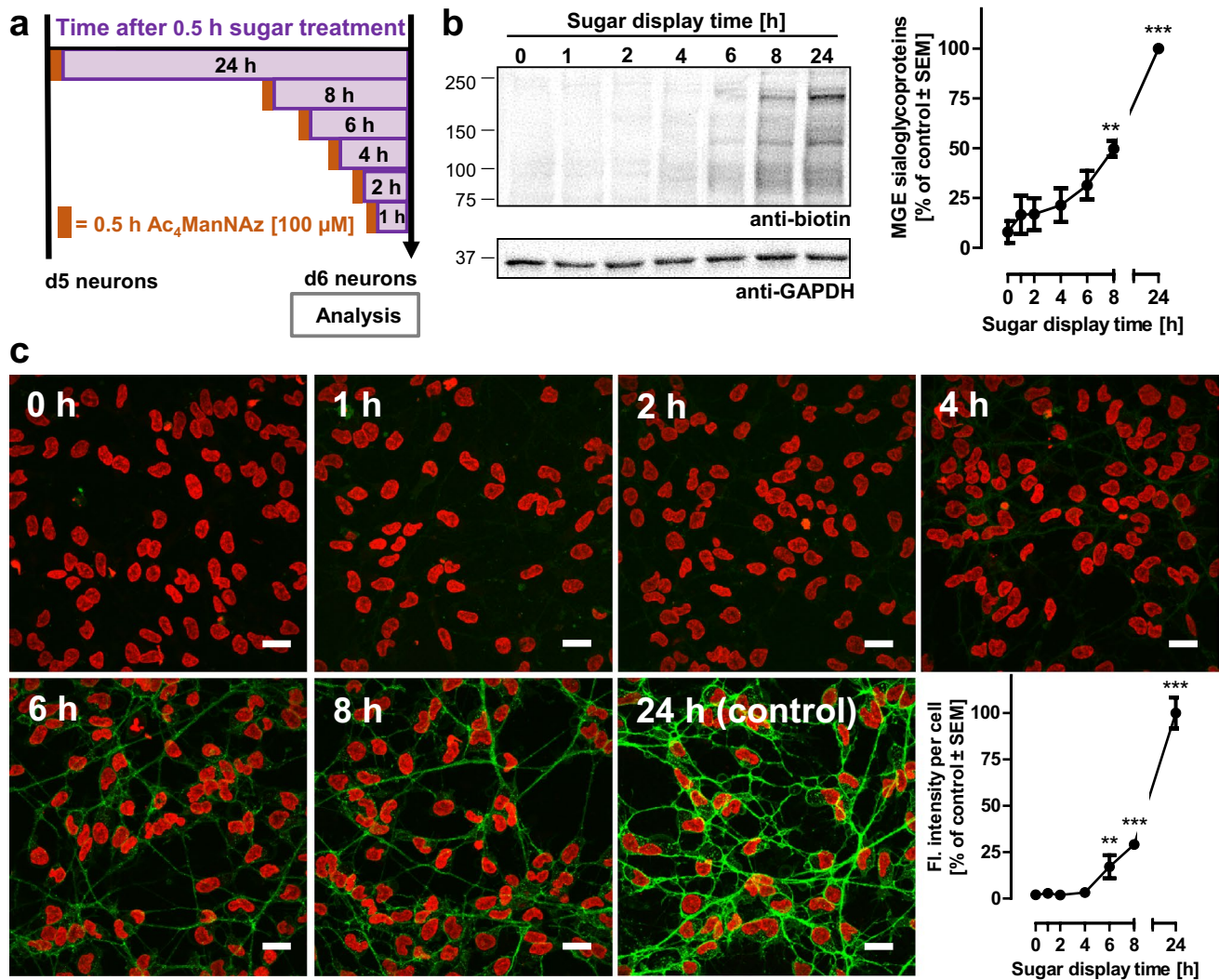
Fig. 5 Time course of cell surface expression of neuronal sialogly-cans. **a** Scheme of experimental setup. LUHMES cells were treated on d5 with Ac$_4$ManNAz [10 µM]. Washing of the sugar, ligation to DBCO-biotin, and visualization by Strep-AF488 were performed at 1, 2, 4, 6, 8, and 24 h after. **b** Quantification of time needed to detect sialoglycoproteins by western blot. MGE sialoglycoproteins, labeled with DBCO-biotin [100 µM] were lyzed and the homogenates were resolved by SDS-PAGE. Western blot against biotin was performed using anti-biotin antibody. For quantifications, lane intensities in the range 75–250 kDa were used. **c** Representative confocal images and fluorescence intensity of MGE sialoglycoconjugates after dif-ferent incorporation times. Images of nuclei stained with H-33342 (red) and MGE sialoglycans visualized by reaction via DBCO-bio-tin followed by Strep-AF488 (green) are merged and presented as maximum z-stack projection with a total z-range of 4 µm. Data are means ± SEM from three independent biological replicates; one-way ANOVA followed by Dunnett's test; **$p < 0.01$, ***$p < 0.001$ (all time points vs. 0 h) Scale bar = 25 µm

The MGE glycoincorporation test (NeuroGlycoTest) to detect early neurofunctional defects

Establishment of the NeuroGlycoTest allowed for a com-parison of three readouts from the same images: live cells, neurite area, and glycoincorporation. To explore the relevant endpoint sensitivities, we selected a small set of tool com-pounds. As standard test setup, differentiated LUHMES were treated with chemicals for a period of 1–24 h and the sugar label (ManNAz) was always added for the last 6 h before the analysis (Fig. 7a). As a control for general cytotoxicity, cells

were treated with the proteasome inhibitor bortezomib. After 24 h exposure, approximately half of the cells had died, as detected by all three endpoint readouts decreased general viability, neurite area, as well as the amount of MGE incor-porated Sia (Fig. 7b).

As cellular surface glycosylation is highly dependent on a functional lipid and protein transport, we used the fungal metabolite brefeldin A to address whether our assay can detect any changes to Sia incorporation when intracellular transport is disrupted. While incubation with brefeldin A for 4 h did not significantly affect general neuronal viability
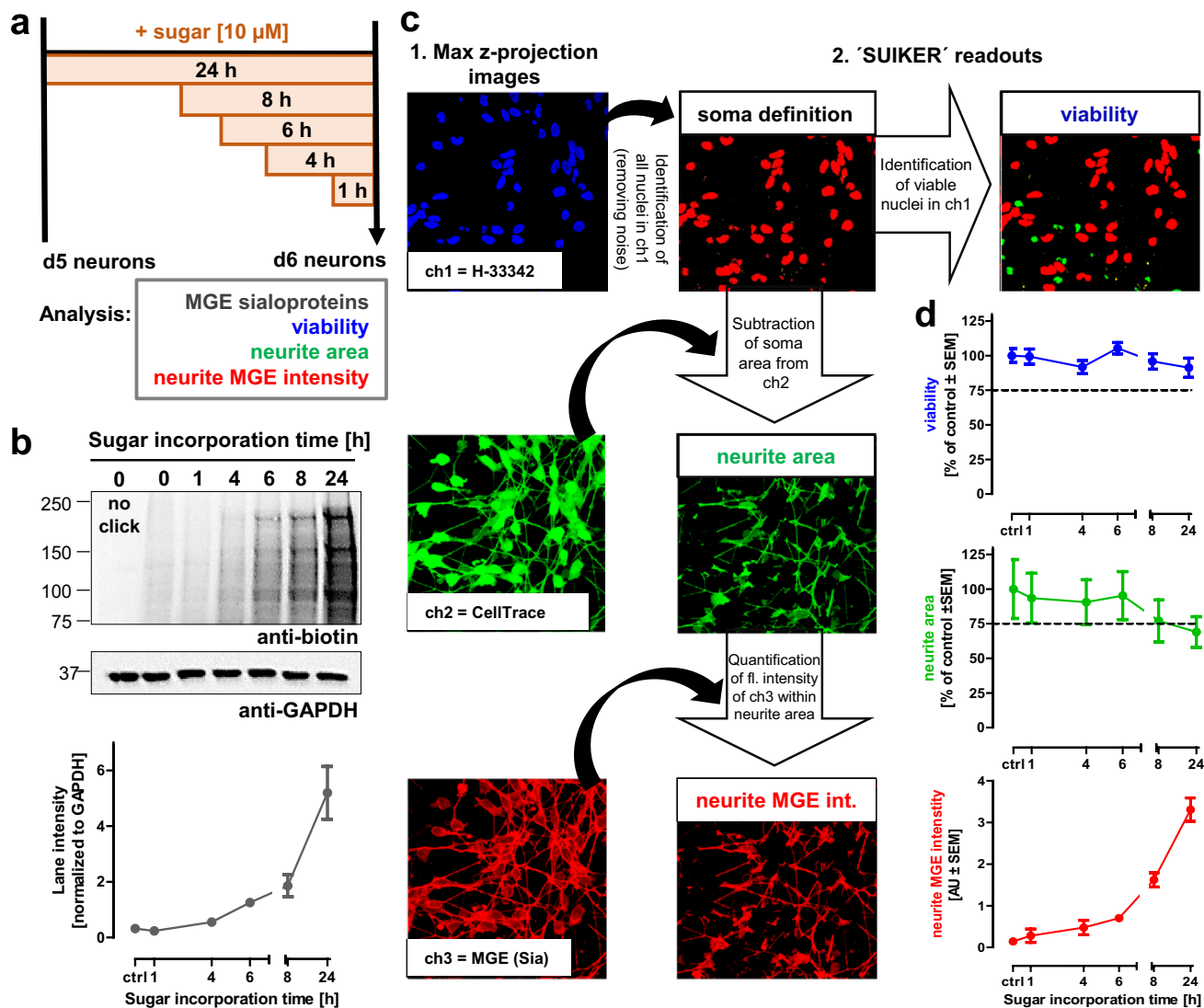
Fig. 6 Features of the SUIKER software used to quantify neurite MGE sialoglycans. **a** Scheme of experimental setup. Differentiated LUHMES cells were treated with Ac₄ManNAz [10 μM] for a duration of 1, 4, 6, 8, and 24 h. After these time points, sugar was washed-off and cells were ligated to DBCO-biotin. Afterwards, cells were either lysed for SDS-PAGE (to determine the amount of MGE sialoglycoproteins) or subsequently stained with a mixture of the nuclear dye H-33342, the vital cytosolic marker CellTrace™ Calcein Red–Orange (=CellTrace) and Strep-AF488 conjugate (to determine the cell surface MGE intensity). **b** Quantification of sialoglycoproteins by western blot. Cells, labeled with DBCO-biotin [100 μM] were lysed and the homogenates were resolved by SDS-PAGE. Western blotting using anti-biotin antibody identified biotinylated proteins. For quantifications, lane intensities in the range 75–250 kDa were used. **c** Principle of the SUIKER software. Representative confocal image shows nuclei in channel 1 (ch1) stained with H-33342 (blue), CellTrace™ Calcein Red–Orange (=CellTrace) stained neurons in channel 2 (ch2) (green), and MGE-labeled sialoglycans in channel 3 (ch3) (red). The image is a merge of nine confocal planes (=single slices) presented as a maximum *z*-stack projection with total range of 4 μm. SUIKER software defines the soma area based on H-33342 nuclear staining from channel 1 (ch1). The viability is assessed by size exclusion of the small non-viable nuclei, while the neurite area is determined via subtraction of all soma area from CellTrace-stained neurons from channel 2 (ch2). Finally, based on MGE labeling from channel 3 (ch3), the labeled Sia fluorescent intensities within neurite area only are quantified, allowing the neurite MGE intensity readout from the same image. **d** Quantification of viability parameters during different sugar incorporation times. Viability in blue, neurite area in green and neurite MGE intensity in red. Data are means ± SEM of seven replicates (color figure online)

or neurite integrity, it almost completely diminished the incorporation of labeled Sia in LUHMES neurites (94% decrease). This was also confirmed by the western blot, where the reduction of sialoglycoprotein levels was obvious

(Fig. 7b, Suppl. Fig. S10). Significant reductions of the neurite integrity by brefeldin A were only observed at 24 h.

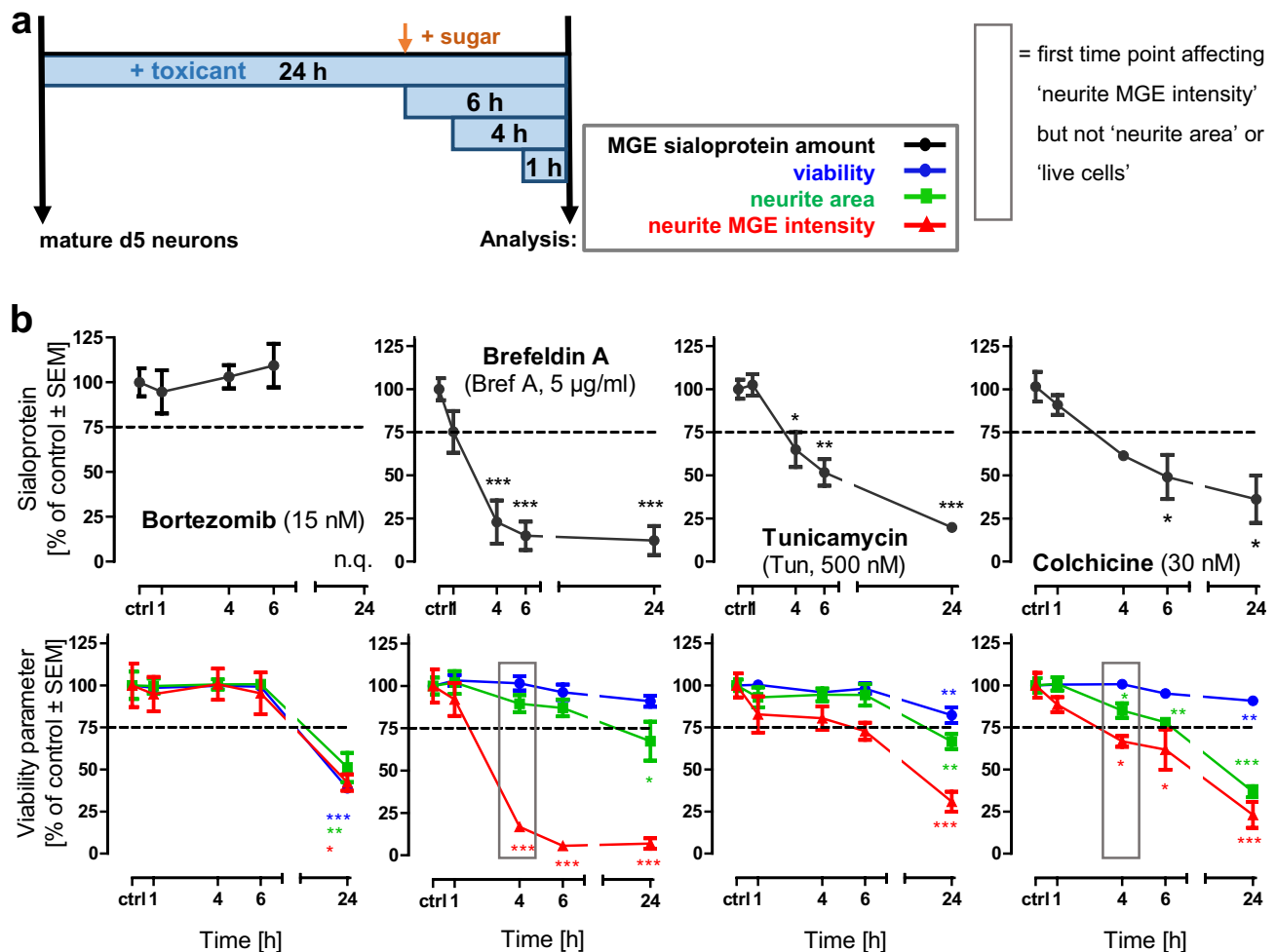Next, we examined the effect of the *N*-glycosylation inhibitor tunicamycin. Here, none of the three viability

Fig. 7 MGE glycoincorporation to detect early neurotoxicity after exposure to tool compounds. **a** Scheme of experimental setup. Differentiated LUHMES cells were treated with toxicants for a duration of 1, 4, 6, and 24 h in a reverse-treatment time protocol. $Ac_4ManNAz$ [10 µM] was added for the last 6 h. Cells were then washed and ligated to DBCO-biotin. Afterwards, cells were either lysed for SDS-PAGE or subsequently stained with a mixture of H-33342, CellTrace™ Calcein Red–Orange (=CellTrace) and fluorescent streptavidin (Strep-AF488). **b** Time-response curves of MGE sialo-glycoprotein amount (black), viability (blue), neurite area (green), and neurite MGE intensity (red) after toxicant treatment. *n.q.* non-quantifiable (for 24 h bortezomib-exposed samples, lack of viable cells made the quantification of MGE incorporated sialoglycoproteins not possible). Data are means $\pm$ SEM from at least three independent biological replicates; one-way ANOVA followed by Dunnett's test; $*p < 0.05$, $**p < 0.01$, $***p < 0.001$ (treated time points vs solvent control) (color figure online)

parameters of the new NeuroGlycoTest was significantly affected at up to 24 h. However, the levels of labeled sialoglycoproteins dropped already at 4 h (Fig. 7b, Suppl. Fig. S10). The stronger effect on protein glycosylation, as compared to overall incorporation of Sia in the glycocalyx is well in line with the known effect of tunicamycin as inhibitor of N-linked protein glycosylation (Esko et al. 2015; Noma et al. 2009; Torre and Steward 1996), but not of lipid glycosylation.

The chemotherapeutic alkaloid colchicine is known to disturb microtubule organization, and therefore also neurite structures (Bonfoco et al. 1996). This compound was selected to illustrate what happens to Sia conjugates once

neurite integrity is impaired. The comparison of all end-points showed that treatment with 30 nM colchicine affects neurite integrity much earlier (4 h) than the general viability (24 h) (Fig. 7b). As expected, the amount of neurite Sia decreased with the decreasing neurite area, also from 4 h onwards. However, Sia also decreased significantly when it was normalized to the reduced neurite area. Moreover, a reduction of MGE sialoglycoproteins was confirmed by western blot (Fig. 7b, Suppl. Fig. S10) in neurons that were still intact.

In summary, these data show that Sia incorporation into neurites is a specific cell proteostasis parameter that can be affected independent of cell viability and neurite growth.

Effect of mitochondrial toxicants on the NeuroGlycoTest readout

A large number of known neurotoxicants targets neurites (Delp et al. 2018b, 2019; Harrill 2018; Narro et al. 2007; Stiegler et al. 2011). Especially, growing neurites are more susceptible to the exposure of neurotoxicants (Krug et al. 2013) (Suppl. Fig. S11), while specific toxicity is hardly seen at all in mature neurons (Delp et al. 2018a). In general, toxicants that are targeting neurites specifically (without loss of general cell viability), reduce or completely lose such specificity (Suppl. Fig. S11).

Encouraged by the high sensitivity of the NeuroGlycoTest, we asked whether neurite changes (in sialylation) could be detected when mature cells are treated with toxicants. This would provide an example of the superiority of the new assay, compared to traditional endpoints (Leist and Hengstler 2018). We exposed differentiated LUHMES to various mitochondrial toxicants for a period of 1–24 h and the sugar was added for the last 6 h before the analysis (Fig. 8a). The concentrations we selected were those that have been previously shown in our laboratory to affect either growing or developed neurites after 24 h exposure (Suppl. Fig. S11).

Antimycin A, a complex III inhibitor of respiratory chain, significantly affected neurites more than viability after 4 h treatment. However, the decrease in the incorporated Sia (by 37%) was observed already after 1 h treatment period, before any effect on neurite area or general viability was detectable (Fig. 8b, Suppl. Fig. S10). An early reduction in neuritial Sia
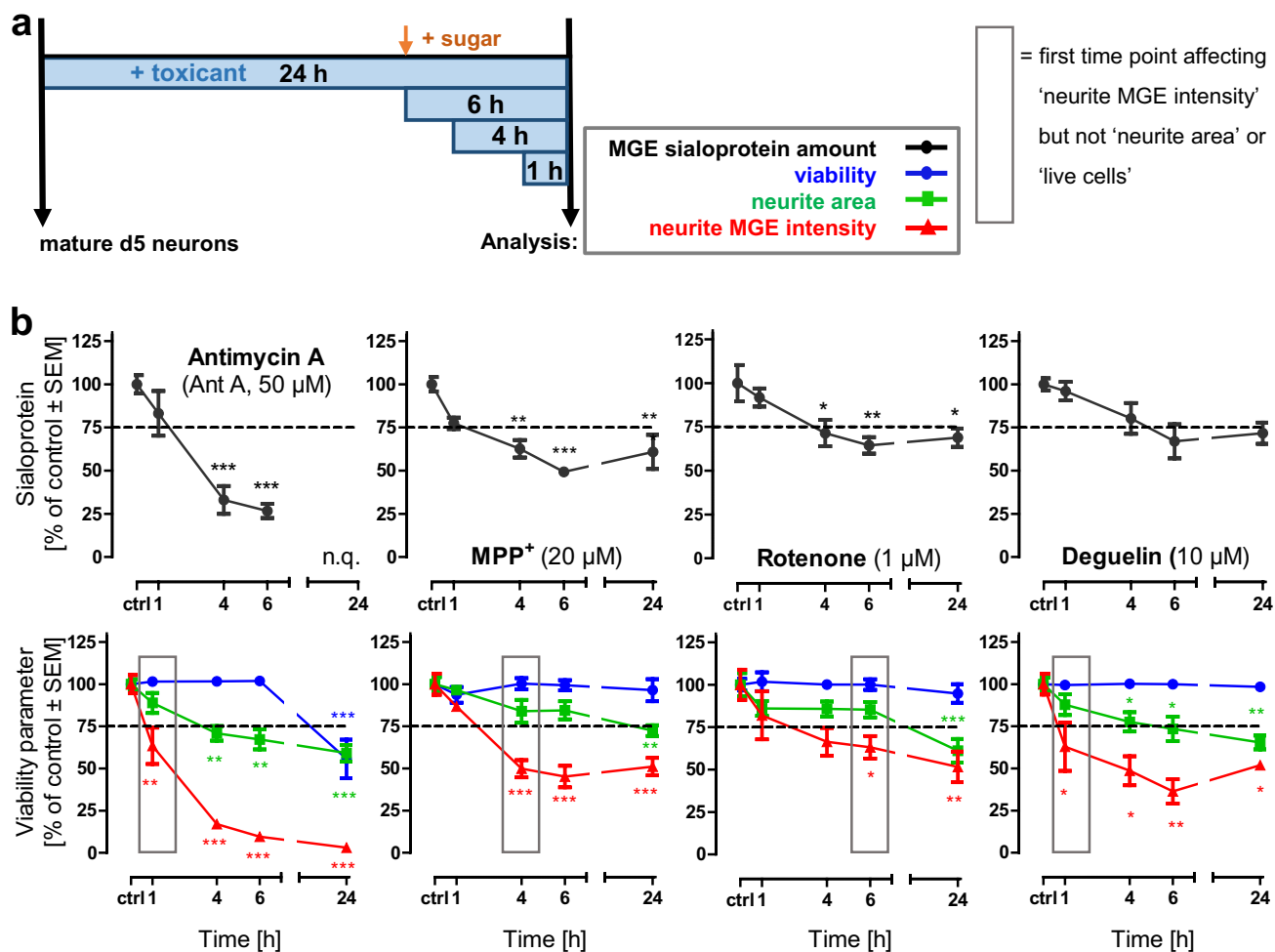

Fig. 8 MGE glycoincorporation to detect early neurotoxicity after exposure to mitochondrial toxicants. **a** Scheme of experimental setup. Differentiated LUHMES cells were treated with toxicants for a duration of 1, 4, 6, and 24 h in a reverse-treatment time protocol. Ac$_4$ManNAz [10 µM] was added for the last 6 h. Cells were then washed and ligated to DBCO-biotin. Afterwards, cells were either lysed for SDS-PAGE or subsequently stained with a mixture of H-33342, CellTrace™ Calcein Red–Orange (=CellTrace) and fluorescent streptavidin (Strep-AF488). **b** Time-response curves of MGE sialoglycoprotein amount (black), viability (blue), neurite area (green), and neurite MGE intensity (red) after toxicant treatment. Data are means ± SEM from at least three independent biological replicates; one-way ANOVA followed by Dunnett's test; *$p < 0.05$, **$p < 0.01$, ***$p < 0.001$ (treated time points vs. solvent control)

was also observed for other mitochondrial respiratory chain disruptors, 1-Methyl-4-phenylpyridinium (MPP$^+$), rotenone and deguelin (Fig. 8b, Suppl. Fig S10). While the integrity of mature neurites remains unaffected until later time points (24 h for MPP$^+$ and rotenone, 4 h for deguelin), a significant decrease of labeled Sia was observed much earlier (4 h for MPP$^+$, 6 h for rotenone, 1 h for deguelin). The general viability remained mostly unaffected (Fig. 8b).

To get an overview of the sequence of events we measured for few compounds (rotenone, MPP$^+$), also cellular ATP content, mitochondrial membrane potential (MMP), cellular respiration, and mitochondrial mobility (Suppl. Fig. S12). The data suggest that the MMP and ATP levels are maintained over a long time (Suppl. Fig. S12a) and their change correlates with structural damage. However, the oxygen consumption rate (OCR; = respiratory chain activity) was affected within minutes of rotenone exposure (Suppl. Fig. S12b). An intermediary step on the time scale are proteostasis disturbances (Terron et al. 2018). For instance, as sialylation and mitochondrial mobility are affected (Suppl. Fig. S12b, c).

Finally, we checked whether such effects would also be observed in other neuronal cells. We generated human peripheral neurons from iPSC (Delp et al. 2018b; Hoelting et al. 2016) and compared MGE labeling with viability effects over time, when the cells were exposed to rotenone. Data were essentially similar to those obtained for LUHMES cells (Suppl. Fig. S13).

These data suggest that the NeuroGlycoTest is able to detect specific effects on neurite glycosylation in the absence of general cytotoxicity and with higher sensitivity compared to neurite area measurements. This assay is therefore a useful novel addition to a battery of tests that are able to pick up alerts for potential neurotoxicants and modifiers of neural function (Bal-Price et al. 2017; Gerhardt et al. 2001; Hansson et al. 2000; Hirt et al. 2000; Ruszkiewicz et al. 2018; Schultz et al. 2015; Tiffany-Castiglioni et al. 2006; Vassallo et al. 2017; Zimmer et al. 2011a, b). Based on the overall results of such a test battery, potential toxicants may be prioritized for further testing (Bal-Price et al. 2018; Li et al. 2019; Schmidt et al. 2017; Smirnova et al. 2014; van Thriel et al. 2012).

Conclusions and outlook

We have demonstrated that reduced incorporation of azide-modified *N*-acetylmannosamine (ManNAz) into Sia of neurites can reveal changes of the neuronal synthesis and sorting of complex biomolecules (Fig. 9). Such subtle functional changes would normally not be detected by readouts of general viability or cell structure (e.g. neurite integrity).

Sia labeling in human neurons was established using an azide-tagged mannosamine analog. We carefully controlled for the cytotoxicity of the unnatural mannosamines in the LUHMES neuronal model and we found that the usual concentrations used to label Sia of most cell lines (50–200 μM) were not suited for neuronal labeling. However, concentrations as low as 10 μM were tolerated well and gave good labeling results. This may be due to the fact that neurons, unlike other cells, contain very high amounts of Sia (Du et al. 2009; Schnaar et al. 2014). A quantitative method of Sia analysis showed that 38% of the natural Sia were replaced with the azide-tagged variant after 24 h. We also found that labeling times of 0.5 h were sufficient in LUHMES neurons and that MGE-labeled Sia was detectable in the glycocalyx as early as 6 h after the modified mannosamine was added to the culture medium. These features of neuronal cultures allow for a high temporal resolution in studies following the fate of newly labeled sialoglycoproteins and lipids.

Glycosylation not only promotes maturation and quality control of proteins in the secretory pathway, but also participates in other key biological processes, including cellular adhesion and signaling, trafficking and clearance of molecules, receptor activation and endocytosis (Moremen et al. 2012; Ohtsubo and Marth 2006; Ungar 2009; Zhang and Wang 2016). Therefore, even slight changes of cellular metabolism or proteostasis may affect the glycosylation patterns on the cellular surface. This feature was used here to establish a particularly sensitive assay for toxicants disturbing mitochondrial function and glycoprotein synthesis. It allows especially the detection of functional deficits early after toxicant application and it complements another new assay for mitotoxicants that uses standard readouts, but alters the composition of the cell culture media by exchanging glucose for galactose (Delp et al. 2019).

As to why mitochondrial toxicants led to such early changes in glycosylation, there can be several explanations. First, glycosylation is an enzymatic process that requires energy in form of ATP and local deficits of trinucleotides may occur even though overall cellular ATP remains unaltered. The biosynthesis of sialic acid-containing complex carbohydrates requires an activated form of sialic acid, CMP-sialic acid. The sialyltransferases are only present in Golgi and only CMP-Sia, not free Sia, can be transported into the Golgi lumen (Munster et al. 1998). Also, the CMP is the substrate of Sia-modifying enzymes. Any dysfunction to the local ATP production (caused by mitochondrial respiratory toxicants) could therefore also lead to decrease of Sia activation and therefore overall sialylation. Alternatively, the block of the respiratory chain may affect glycosylation and transport of glycoconjugates in an energy independent form (Krug et al. 2014; Poltl et al. 2012). A typical
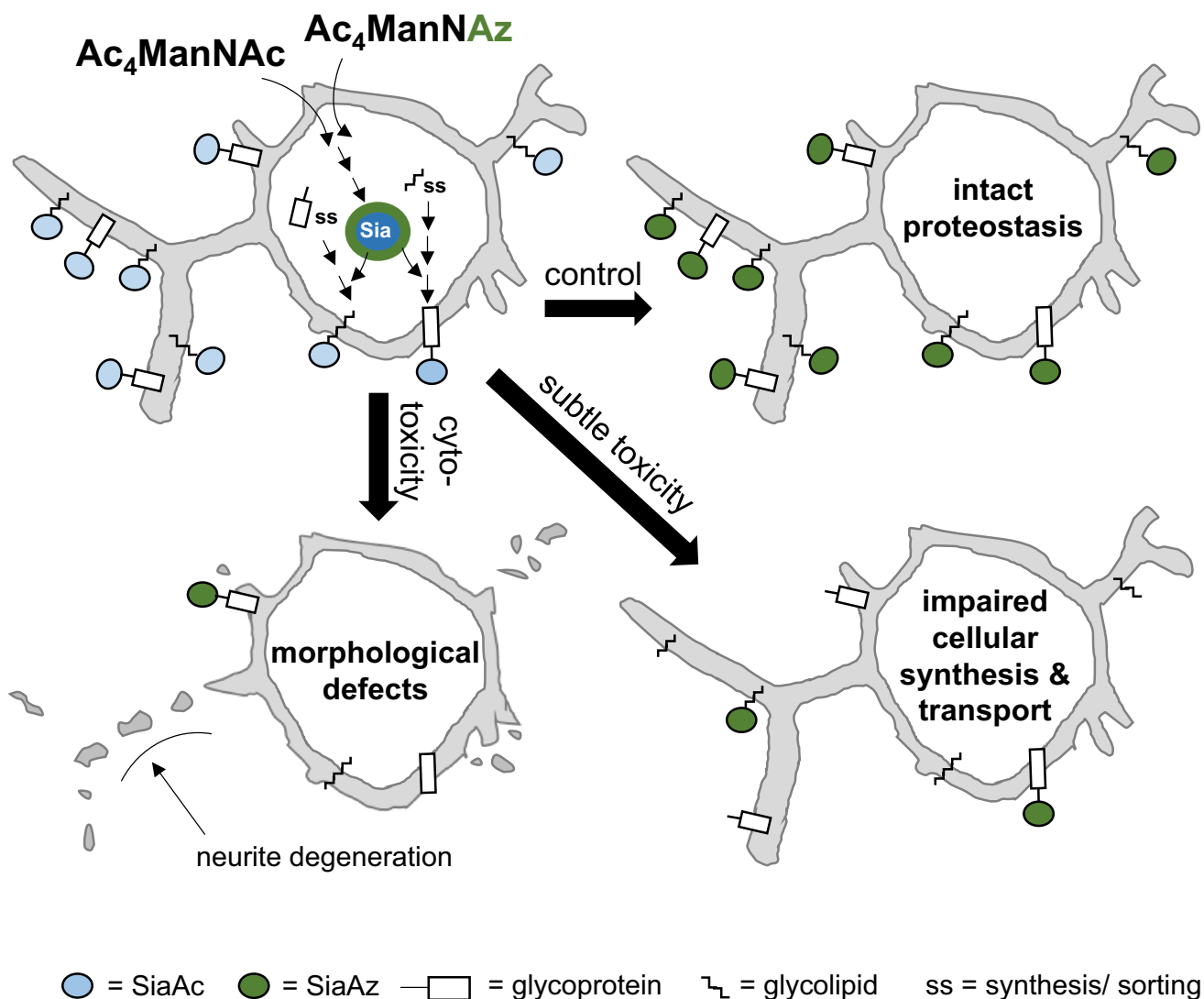
Fig. 9 Subtle toxicity detection by ManNAz incorporation rate into neurites. Schematic illustration of potential effects of toxicant treatments on the fate of Sia-coupled biomolecules usually localized to cell membranes. Neurons accept the azide-tagged mannosamine (Ac$_4$ManNAz) and incorporate it into the Sia (Sia) attached to newly synthesized and sorted (=ss) glycoproteins and glycolipids. These are then transported to the cellular plasma membrane. In a healthy neuron with an intact proteostasis, the azide-tagged Sia (green) will be displayed throughout the whole neuronal plasma membrane. Any subtle toxicity leading to disturbed cellular synthesis and transport will be reflected by a reduction of the incorporated Sia before. Such functional impairments may occur independent of structural damage, prior to structural damage or simultaneously with structural damage/ neurite degeneration

Sia-containing glycoprotein—mucin has also been shown to act like an ·OH scavenger when sialylated (Ogasawara et al. 2007). One could therefore hypothesize that the decrease in Sia during mitochondrial stress, like in our study, may be a result of most of the Sia being destroyed by scavenging the increased ROS during the oxidative stress. Moreover, the increased oxidative stress has been associated with an increase in sialidase activity (Wei and Wang 2019), which means less Sia linked to proteins and lipids.

The high sensitivity of the NeuroGlycoTest developed here was shown by comparing it to other viability measurements such as general neuronal viability and neurite integrity readouts. Testing the effect of several model compounds in the NeuroGlycoTest revealed that the incorporation of MGE-labeled Sia into LUHMES neurites can serve as a highly sensitive assay to identify compounds that affect glycosylation levels, when (1) neurites are disturbed early (colchicine) or when (2) neurites are disturbed late (brefeldin A, tunicamycin).

In summary, the NeuroGlycoTest is suited as a screen to identify compounds causing subtle neuronal toxicity by affecting biosynthesis pathway. It is an important step toward more sensitive detection of neurotoxicants. However, it may also be used in future to characterize drug candidates

designed to disturb certain biosynthesis processes related to glycosylated biomolecules.

Author contributions PK designed and performed most of the experiments, analyzed data, and wrote the manuscript; CK developed the SUIKER image analysis software and the western blot image evaluation software; AK, MF, A-KH, and SK designed and performed experiments, JN and SH helped with the plug in for Fiji image processing; JD designed and performed experiments and proofread the manuscript; VW designed experiments and proofread the manuscript; ML designed experiments and wrote the manuscript.

Compliance with ethical standards

Conflict of interest The authors declare that they have no conflict of interest.

References

Aebi M, Bernasconi R, Clerc S, Molinari M (2010) *N*-glycan structures: recognition and processing in the ER. Trends Biochem Sci 35(2):74–82. https://doi.org/10.1016/j.tibs.2009.10.001

Almaraz RT, Aich U, Khanna HS et al (2012) Metabolic oligosaccharide engineering with *N*-Acyl functionalized ManNAc analogs: cytotoxicity, metabolic flux, and glycan-display considerations. Biotechnol Bioeng 109(4):992–1006. https://doi.org/10.1002/bit.24363

Axelsson V, Holback S, Sjogren M, Gustafsson H, Forsby A (2006) Gliotoxin induces caspase-dependent neurite degeneration and calpain-mediated general cytotoxicity in differentiated human neuroblastoma SH-SY5Y cells. Biochem Biophys Res Commun 345(3):1068–1074. https://doi.org/10.1016/j.bbrc.2006.05.019

Bal-Price A, Lein PJ, Keil KP et al (2017) Developing and applying the adverse outcome pathway concept for understanding and predicting neurotoxicity. Neurotoxicology 59:240–255. https://doi.org/10.1016/j.neuro.2016.05.010

Bal-Price A, Hogberg HT, Crofton KM et al (2018) Recommendation on test readiness criteria for new approach methods in toxicology: exemplified for developmental neurotoxicity. Altex 35(3):306–352. https://doi.org/10.14573/altex.1712081

Bonfoco E, Leist M, Zhivotovsky B, Orrenius S, Lipton SA, Nicotera P (1996) Cytoskeletal breakdown and apoptosis elicited by NO donors in cerebellar granule cells require NMDA receptor activation. J Neurochem 67(6):2484–2493. https://doi.org/10.1046/j.1471-4159.1996.67062484.x

Buttner B, Kannicht C, Schmidt C et al (2002) Biochemical engineering of cell surface sialic acids stimulates axonal growth. J Neurosci 22(20):8869–8875

Campbell CT, Sampathkumar SG, Yarema KJ (2007) Metabolic oligosaccharide engineering: perspectives, applications, and future directions. Mol Biosyst 3(3):187–194. https://doi.org/10.1039/b614939c

Ceresa C, Avan A, Giovannetti E et al (2014) Characterization of and protection from neurotoxicity induced by oxaliplatin, bortezomib and epothilone-B. Anticancer Res 34(1):517–523

Charter NW, Mahal LK, Koshland DE Jr, Bertozzi CR (2000) Biosynthetic incorporation of unnatural sialic acids into polysialic acid on neural cells. Glycobiology 10(10):1049–1056

Charter NW, Mahal LK, Koshland DE Jr, Bertozzi CR (2002) Differential effects of unnatural sialic acids on the polysialylation of the neural cell adhesion molecule and neuronal behavior. J Biol Chem 277(11):9255–9261. https://doi.org/10.1074/jbc.M111619200

Culbreth ME, Harrill JA, Freudenrich TM, Mundy WR, Shafer TJ (2012) Comparison of chemical-induced changes in proliferation and apoptosis in human and mouse neuroprogenitor cells. Neurotoxicology 33(6):1499–1510. https://doi.org/10.1016/j.neuro.2012.05.012

Delp J, Gutbier S, Cerff M et al (2018a) Stage-specific metabolic features of differentiating neurons: Implications for toxicant sensitivity. Toxicol Appl Pharmacol 354:64–80. https://doi.org/10.1016/j.taap.2017.12.013

Delp J, Gutbier S, Klima S et al (2018b) A high-throughput approach to identify specific neurotoxicants/ developmental toxicants in human neuronal cell function assays. Altex 35(2):235–253. https://doi.org/10.14573/altex.1712182

Delp J, Funke M, Rudolf F et al (2019) Development of a neurotoxicity assay that is tuned to detect mitochondrial toxicants. Arch Toxicol. https://doi.org/10.1007/s00204-019-02473-y

Dennis JW, Nabi IR, Demetriou M (2009) Metabolism, cell surface organization, and disease. Cell 139(7):1229–1241. https://doi.org/10.1016/j.cell.2009.12.008

Dold J, Pfotzer J, Spate AK, Wittmann V (2017) Dienophile-modified mannosamine derivatives for metabolic labeling of sialic acids: a comparative study. ChemBioChem 18(13):1242–1250. https://doi.org/10.1002/cbic.201700002

Doll F, Buntz A, Spate AK et al (2016) Visualization of protein-specific glycosylation inside living cells. Angew Chem Int Ed Engl 55(6):2262–2266. https://doi.org/10.1002/anie.201503183

Du J, Meledeo MA, Wang Z, Khanna HS, Paruchuri VD, Yarema KJ (2009) Metabolic glycoengineering: sialic acid and beyond. Glycobiology 19(12):1382–1401. https://doi.org/10.1093/glycob/cwp115

Dube DH, Bertozzi CR (2003) Metabolic oligosaccharide engineering as a tool for glycobiology. Curr Opin Chem Biol 7(5):616–625

Efremova L, Chovancova P, Adam M, Gutbier S, Schildknecht S, Leist M (2017) Switching from astrocytic neuroprotection to neurodegeneration by cytokine stimulation. Arch Toxicol 91(1):231–246. https://doi.org/10.1007/s00204-016-1702-2

Esko JD, Bertozzi C, Schnaar RL (2015) Chemical tools for inhibiting glycosylation. In: rd, Varki A, Cummings RD, et al. (eds) Essentials of glycobiology. Cold Spring Harbor (NY), p 701–712. https://doi.org/10.1101/glycobiology.3e.055

Flaskos J, Nikolaidis E, Harris W, Sachana M, Hargreaves AJ (2011) Effects of sub-lethal neurite outgrowth inhibitory concentrations of chlorpyrifos oxon on cytoskeletal proteins and acetylcholinesterase in differentiating N2a cells. Toxicol Appl Pharmacol 256(3):330–336. https://doi.org/10.1016/j.taap.2011.06.002

Frimat JP, Sisnaiske J, Subbiah S et al (2010) The network formation assay: a spatially standardized neurite outgrowth analytical display for neurotoxicity screening. Lab Chip 10(6):701–709. https://doi.org/10.1039/b922193j

Galuska SP, Rollenhagen M, Kaup M et al (2010) Synaptic cell adhesion molecule SynCAM 1 is a target for polysialylation in postnatal mouse brain. Proc Natl Acad Sci USA 107(22):10250–10255. https://doi.org/10.1073/pnas.0912103107

Ganjam GK, Bolte K, Matschke LA et al (2019) Mitochondrial damage by alpha-synuclein causes cell death in human dopaminergic neurons. Cell Death Dis 10(11):865. https://doi.org/10.1038/s41419-019-2091-2

Gerhardt E, Kugler S, Leist M et al (2001) Cascade of caspase activation in potassium-deprived cerebellar granule neurons: targets for treatment with peptide and protein inhibitors of apoptosis. Mol Cell Neurosci 17(4):717–731. https://doi.org/10.1006/mcne.2001.0962

Hansson O, Castilho RF, Kaminski Schierle GS et al (2000) Additive effects of caspase inhibitor and lazaroid on the survival of transplanted rat and human embryonic dopamine neurons. Exp Neurol 164(1):102–111. https://doi.org/10.1006/exnr.2000.7406

Harrill JA (2018) Human-derived neurons and neural progenitor cells in high content imaging applications. Methods Mol Biol 1683:305–338. https://doi.org/10.1007/978-1-4939-7357-6_18

Harris G, Eschment M, Orozco SP et al (2018) Toxicity, recovery, and resilience in a 3D dopaminergic neuronal in vitro model exposed to rotenone. Arch Toxicol 92(8):2587–2606. https://doi.org/10.1007/s00204-018-2250-8

Hebert DN, Garman SC, Molinari M (2005) The glycan code of the endoplasmic reticulum: asparagine-linked carbohydrates as protein maturation and quality-control tags. Trends Cell Biol 15(7):364–370. https://doi.org/10.1016/j.tcb.2005.05.007

Hirt UA, Gantner F, Leist M (2000) Phagocytosis of nonapoptotic cells dying by caspase-independent mechanisms. J Immunol 164(12):6520–6529. https://doi.org/10.4049/jimmunol.164.12.6520

Hoelting L, Klima S, Karreman C et al (2016) Stem cell-derived immature human dorsal root ganglia neurons to identify peripheral neurotoxicants. Stem Cells Transl Med 5(4):476–487. https://doi.org/10.5966/sctm.2015-0108

Kang K, Joo S, Choi JY et al (2015) Tissue-based metabolic labeling of polysialic acids in living primary hippocampal neurons. Proc Natl Acad Sci USA 112(3):E241–E248. https://doi.org/10.1073/pnas.1419683112

Karreman C, Kranaster P, Leist M (2019) SUIKER: quantification of antigens in cell organelles, neurites and cellular sub-structures by imaging. Altex 36(3):518–520. https://doi.org/10.14573/altex.1906251

Keppler OT, Horstkorte R, Pawlita M, Schmidt C, Reutter W (2001) Biochemical engineering of the N-acyl side chain of sialic acid: biological implications. Glycobiology 11(2):11R–18R. https://doi.org/10.1093/glycob/11.2.11r

Krug AK, Balmer NV, Matt F, Schonenberger F, Merhof D, Leist M (2013) Evaluation of a human neurite growth assay as specific screen for developmental neurotoxicants. Arch Toxicol 87(12):2215–2231. https://doi.org/10.1007/s00204-013-1072-y

Krug AK, Gutbier S, Zhao L et al (2014) Transcriptional and metabolic adaptation of human neurons to the mitochondrial toxicant MPP(+). Cell Death Dis 5:e1222. https://doi.org/10.1038/cddis.2014.166

Lau KS, Partridge EA, Grigorian A et al (2007) Complex N-glycan number and degree of branching cooperate to regulate cell proliferation and differentiation. Cell 129(1):123–134. https://doi.org/10.1016/j.cell.2007.01.049

Laughlin ST, Bertozzi CR (2007) Metabolic labeling of glycans with azido sugars and subsequent glycan-profiling and visualization via Staudinger ligation. Nat Protoc 2(11):2930–2944. https://doi.org/10.1038/nprot.2007.422

Leist M, Hengstler JG (2018) Essential components of methods papers. Altex 35(3):429–432. https://doi.org/10.14573/altex.1807031

Leist M, Jaattela M (2001) Four deaths and a funeral: from caspases to alternative mechanisms. Nat Rev Mol Cell Biol 2(8):589–598. https://doi.org/10.1038/35085008

Leist M, Nicotera P (1998) Calcium and neuronal death. Rev Physiol Biochem Pharmacol 132:79–125

Li J, Settivari R, LeBaron MJ, Marty MS (2019) An industry perspective: a streamlined screening strategy using alternative models for chemical assessment of developmental neurotoxicity. Neurotoxicology 73:17–30. https://doi.org/10.1016/j.neuro.2019.02.010

Merzaban JS, Imitola J, Starossom SC et al (2015) Cell surface glycan engineering of neural stem cells augments neurotropism and improves recovery in a murine model of multiple sclerosis. Glycobiology 25(12):1392–1409. https://doi.org/10.1093/glycob/cwv046

Moremen KW, Tiemeyer M, Nairn AV (2012) Vertebrate protein glycosylation: diversity, synthesis and function. Nat Rev Mol Cell Biol 13(7):448–462. https://doi.org/10.1038/nrm3383

Muhlenhoff M, Rollenhagen M, Werneburg S, Gerardy-Schahn R, Hildebrandt H (2013) Polysialic acid: versatile modification of NCAM, SynCAM 1 and neuropilin-2. Neurochem Res 38(6):1134–1143. https://doi.org/10.1007/s11064-013-0979-2

Munster AK, Eckhardt M, Potvin B, Muhlenhoff M, Stanley P, Gerardy-Schahn R (1998) Mammalian cytidine 5'-monophosphate N-acetylneuraminic acid synthetase: a nuclear protein with evolutionarily conserved structural motifs. Proc Natl Acad Sci USA 95(16):9140–9145. https://doi.org/10.1073/pnas.95.16.9140

Narro ML, Yang F, Kraft R, Wenk C, Efrat A, Restifo LL (2007) NeuronMetrics: software for semi-automated processing of cultured neuron images. Brain Res 1138:57–75. https://doi.org/10.1016/j.brainres.2006.10.094

Niederwieser A, Spate AK, Nguyen LD, Jungst C, Reutter W, Wittmann V (2013) Two-color glycan labeling of live cells by a combination of Diels–Alder and click chemistry. Angew Chem Int Ed Engl 52(15):4265–4268. https://doi.org/10.1002/anie.201208991

Nischan N, Kohler JJ (2016) Advances in cell surface glycoengineering reveal biological function. Glycobiology 26(8):789–796. https://doi.org/10.1093/glycob/cww045

Noma K, Kimura K, Minatohara K et al (2009) Triple N-glycosylation in the long S5-P loop regulates the activation and trafficking of the Kv12.2 potassium channel. J Biol Chem 284(48):33139–33150. https://doi.org/10.1074/jbc.M109.021519

Ogasawara Y, Namai T, Yoshino F, Lee MC, Ishii K (2007) Sialic acid is an essential moiety of mucin as a hydroxyl radical scavenger. FEBS Lett 581(13):2473–2477. https://doi.org/10.1016/j.febslet.2007.04.062

Ohtsubo K, Marth JD (2006) Glycosylation in cellular mechanisms of health and disease. Cell 126(5):855–867. https://doi.org/10.1016/j.cell.2006.08.019

Pham ND, Fermaintt CS, Rodriguez AC, McCombs JE, Nischan N, Kohler JJ (2015) Cellular metabolism of unnatural sialic acid precursors. Glycoconj J 32(7):515–529. https://doi.org/10.1007/s10719-015-9593-7

Poltl D, Schildknecht S, Karreman C, Leist M (2012) Uncoupling of ATP-depletion and cell death in human dopaminergic neurons. Neurotoxicology 33(4):769–779. https://doi.org/10.1016/j.neuro.2011.12.007

Ruszkiewicz JA, Pinkas A, Miah MR et al (2018) C. elegans as a model in developmental neurotoxicology. Toxicol Appl Pharmacol 354:126–135. https://doi.org/10.1016/j.taap.2018.03.016

Saxena S, Caroni P (2007) Mechanisms of axon degeneration: from development to disease. Prog Neurobiol 83(3):174–191. https://doi.org/10.1016/j.pneurobio.2007.07.007

Saxon E, Bertozzi CR (2000) Cell surface engineering by a modified Staudinger reaction. Science 287(5460):2007–2010. https://doi.org/10.1126/science.287.5460.2007

Saxon E, Luchansky SJ, Hang HC, Yu C, Lee SC, Bertozzi CR (2002) Investigating cellular metabolism of synthetic azidosugars with the Staudinger ligation. J Am Chem Soc 124(50):14893–14902. https://doi.org/10.1021/ja027748x

Schildknecht S, Karreman C, Poltl D et al (2013) Generation of genetically-modified human differentiated cells for toxicological tests and the study of neurodegenerative diseases. Altex 30(4):427–444. https://doi.org/10.14573/altex.2013.4.427

Schmidt C, Stehling P, Schnitzer J, Reutter W, Horstkorte R (1998) Biochemical engineering of neural cell surfaces by the synthetic N-propanoyl-substituted neuraminic acid precursor. J Biol Chem 273(30):19146–19152

Schmidt BZ, Lehmann M, Gutbier S et al (2017) In vitro acute and developmental neurotoxicity screening: an overview of cellular platforms and high-throughput technical possibilities. Arch Toxicol 91(1):1–33. https://doi.org/10.1007/s00204-016-1805-9

Schnaar RL, Gerardy-Schahn R, Hildebrandt H (2014) Sialic acids in the brain: gangliosides and polysialic acid in nervous system development, stability, disease, and regeneration. Physiol Rev 94(2):461–518. https://doi.org/10.1152/physrev.00033.2013

Scholz D, Poltl D, Genewsky A et al (2011) Rapid, complete and large-scale generation of post-mitotic neurons from the human LUHMES cell line. J Neurochem 119(5):957–971. https://doi.org/10.1111/j.1471-4159.2011.07255.x

Schultz L, Zurich MG, Culot M et al (2015) Evaluation of drug-induced neurotoxicity based on metabolomics, proteomics and electrical activity measurements in complementary CNS in vitro models. Toxicol In Vitro 30(1 Pt A):138–165. https://doi.org/10.1016/j.tiv.2015.05.016

Singh N, Lawana V, Luo J et al (2018) Organophosphate pesticide chlorpyrifos impairs STAT1 signaling to induce dopaminergic neurotoxicity: Implications for mitochondria mediated oxidative stress signaling events. Neurobiol Dis 117:82–113. https://doi.org/10.1016/j.nbd.2018.05.019

Skirzewski M, Karavanova I, Shamir A et al (2018) ErbB4 signaling in dopaminergic axonal projections increases extracellular dopamine levels and regulates spatial/working memory behaviors. Mol Psychiatry 23(11):2227–2237. https://doi.org/10.1038/mp.2017.132

Sletten EM, Bertozzi CR (2009) Bioorthogonal chemistry: fishing for selectivity in a sea of functionality. Angew Chem Int Ed Engl 48(38):6974–6998. https://doi.org/10.1002/anie.200900942

Smirnova L, Hogberg HT, Leist M, Hartung T (2014) Developmental neurotoxicity—challenges in the 21st century and in vitro opportunities. Altex 31(2):129–156. https://doi.org/10.14573/altex.1403271

Stiegler NV, Krug AK, Matt F, Leist M (2011) Assessment of chemical-induced impairment of human neurite outgrowth by multiparametric live cell imaging in high-density cultures. Toxicol Sci 121(1):73–87. https://doi.org/10.1093/toxsci/kfr034

Terron A, Bal-Price A, Paini A et al (2018) An adverse outcome pathway for parkinsonian motor deficits associated with mitochondrial complex I inhibition. Arch Toxicol 92(1):41–82. https://doi.org/10.1007/s00204-017-2133-4

Tiffany-Castiglioni E, Hong S, Qian Y, Tang Y, Donnelly KC (2006) In vitro models for assessing neurotoxicity of mixtures. Neurotoxicology 27(5):835–839. https://doi.org/10.1016/j.neuro.2006.05.010

Tong ZB, Hogberg H, Kuo D et al (2017) Characterization of three human cell line models for high-throughput neuronal cytotoxicity screening. J Appl Toxicol 37(2):167–180. https://doi.org/10.1002/jat.3334

Tong ZB, Huang R, Wang Y et al (2018) The toxmatrix: chemogenomic profiling identifies interactions that reveal mechanisms of toxicity. Chem Res Toxicol 31(2):127–136. https://doi.org/10.1021/acs.chemrestox.7b00290

Torre ER, Steward O (1996) Protein synthesis within dendrites: glycosylation of newly synthesized proteins in dendrites of hippocampal neurons in culture. J Neurosci 16(19):5967–5978

Ungar D (2009) Golgi linked protein glycosylation and associated diseases. Semin Cell Dev Biol 20(7):762–769. https://doi.org/10.1016/j.semcdb.2009.03.004

van Thriel C, Westerink RH, Beste C, Bale AS, Lein PJ, Leist M (2012) Translating neurobehavioural endpoints of developmental neurotoxicity tests into in vitro assays and readouts. Neurotoxicology 33(4):911–924. https://doi.org/10.1016/j.neuro.2011.10.002

Vassallo A, Chiappalone M, De Camargos LR et al (2017) A multi-laboratory evaluation of microelectrode array-based measurements of neural network activity for acute neurotoxicity testing. Neurotoxicology 60:280–292. https://doi.org/10.1016/j.neuro.2016.03.019

Vogt J, Glumm R, Schluter L et al (2012) Homeostatic regulation of NCAM polysialylation is critical for correct synaptic targeting. Cell Mol Life Sci 69(7):1179–1191. https://doi.org/10.1007/s00018-011-0868-2

Wei M, Wang PG (2019) Desialylation in physiological and pathological processes: new target for diagnostic and therapeutic development. Prog Mol Biol Transl Sci 162:25–57. https://doi.org/10.1016/bs.pmbts.2018.12.001

Wu X, Majumder A, Webb R, Stice SL (2016) High content imaging quantification of multiple in vitro human neurogenesis events after neurotoxin exposure. BMC Pharmacol Toxicol 17(1):62. https://doi.org/10.1186/s40360-016-0107-4

Yoo SW, Motari MG, Susuki K et al (2015) Sialylation regulates brain structure and function. FASEB J 29(7):3040–3053. https://doi.org/10.1096/fj.15-270983

Zhang X, Wang Y (2016) Glycosylation quality control by the golgi structure. J Mol Biol 428(16):3183–3193. https://doi.org/10.1016/j.jmb.2016.02.030

Zimmer B, Kuegler PB, Baudis B et al (2011a) Coordinated waves of gene expression during neuronal differentiation of embryonic stem cells as basis for novel approaches to developmental neurotoxicity testing. Cell Death Differ 18(3):383–395. https://doi.org/10.1038/cdd.2010.109

Zimmer B, Schildknecht S, Kuegler PB, Tanavde V, Kadereit S, Leist M (2011b) Sensitivity of dopaminergic neuron differentiation from stem cells to chronic low-dose methylmercury exposure. Toxicol Sci 121(2):357–367. https://doi.org/10.1093/toxsci/kfr054